Microscopic description of fission in uranium isotopes with the Gogny energy density functional

R. Rodríguez-Guzmán*
Department of Physics and Astronomy, Rice University, Houston, Texas 77005, USA
and Department of Chemistry, Rice University, Houston, Texas 77005, USA

L. M. Robledo†
Departamento de Física Teórica, Universidad Autónoma de Madrid, 28049 Madrid, Spain
(Received 27 December 2013; revised manuscript received 28 March 2014; published 8 May 2014)

The most recent parametrizations D1S, D1N, and D1M of the Gogny energy density functional are used to describe fission in the isotopes $^{232-280}$U. Fission paths, collective masses, and zero-point quantum corrections, obtained within the constrained Hartree-Fock-Bogoliubov approximation, are used to compute the systematics of the spontaneous fission half-lives t_{SF}, the masses and charges of the fission fragments, and their intrinsic shapes. The Gogny-D1M parametrization has been benchmarked against available experimental data on inner and second barrier heights, excitation energies of the fission isomers, and half-lives in a selected set of Pu, Cm, Cf, Fm, No, Rf, Sg, Hs, and Fl nuclei. It is concluded that D1M represents a reasonable starting point to describe fission in heavy and superheavy nuclei. Special attention is also paid to understand the uncertainties in the predicted t_{SF} values arising from the different building blocks entering the standard semiclassical Wentzel-Kramers-Brillouin formula. Although the uncertainties are large, the trend with mass or neutron numbers are well reproduced and therefore the theory still has predictive power. In this respect, it is also shown that modifications of a few percent in the pairing strength can have a significant impact on the collective masses leading to uncertainties in the t_{SF} values of several orders of magnitude.

DOI: 10.1103/PhysRevC.89.054310 PACS number(s): 24.75.+i, 25.85.Ca, 21.60.Jz, 27.90.+b

I. INTRODUCTION

Nuclear fission is, at the same time, one of the most distinctive phenomena in the physics of the nucleus and one of the most elusive to a theoretical description. It takes place mostly in heavy and superheavy nuclei and involves the evolution of the initial parent system from its ground state to scission through a sequence of intrinsic shapes labeled by some sort of deformation parameter [1–3]. Once the scission configuration is reached, the system splits into two daughter nuclei. The occurrence of fission is the result of the competition between the nuclear surface energy coming from the strong interaction and the Coulomb repulsion of the nuclear charge density [4]. In fact, nuclear fission was originally described [4,5] in terms of the liquid-drop model where the surface tension plays an essential role. However, experimental and theoretical evidences emphasize the stabilizing role of shell effects [6–8] and therefore much effort has been given to the development of models that incorporate those effects to the semiclassical liquid-drop model description [9–11]. The outcome of these models (see, for example, Refs. [12,13] and references therein) is a potential energy surface, expressed in terms of several deformation parameters, showing a quite involved topography (direct consequence of shell effects) with minima, valleys, ridges, and saddle points. In this picture, fission is the journey along this complicated landscape from the ground state to the scission point (an elusive concept to be discussed later). In spite of their success in describing some fission observables, these models lack essential quantum mechanisms like tunneling through a classically forbidden barrier or a sound description of the inertia associated with the collective degrees of freedom used to describe fission.

From a more fundamental point of view, fission could be regarded as a quantum mechanical problem describing the evolution from some given initial quantum state to a final state with two fragments and involving tunneling through a potential barrier defined in a multidimensional space. The initial state can be the parent nucleus ground state in spontaneous fission or a highly excited state (usually described as a statistical admixture by assuming thermal equilibrium) in induced fission. Although several attempts to deal with this problem in a path-integral framework involving instantons and other sophisticated concepts have been considered [14,15] in the past, it has not been possible to establish a computationally feasible framework capable to describe real nuclei with realistic interactions. Therefore, it is customary to use a more phenomenological approach where the dynamical changes involved in the transition from a single nucleus to two fragments are usually described in the framework of the (constrained) self-consistent mean-field approximation [6,16] based on a given nonrelativistic energy density functional (EDF) of the Gogny [17–25] and/or Skyrme [26–31] type, as well as with several parametrizations of the relativistic mean-field (RMF) Lagrangian [32–36]. Recently, the fission properties of the Barcelona-Catania-Paris-Madrid (BCPM) EDF [37] have also been studied in the case of drip-line-to-drip-line uranium isotopes [38]. The aim of all these methods is to determine the relevant fission configurations by means of the Hartree-Fock-Bogoliubov (HFB) mean-field method using constraints on relevant quantities associated with

*raynerrobertorodriguez@gmail.com
†luis.robledo@uam.es

shape parameters like multipole moments or neck degrees of freedom. The resulting HFB wave functions are then used to compute other parameters like the collective inertia and quantum corrections to the potential energy surface stemming from the restoration of broken symmetries (rotational, parity, etc.) and fluctuations in the collective parameters defining the fission paths. An implicit assumption of this framework is that the fission properties are determined by general features of the interactions and therefore no fine tuning should be required to describe fission observables. However, interactions are usually tuned to reproduce nuclear matter parameters that are not properly constrained by experimental data (the typical case pertaining fission is the surface energy of semi-infinite nuclear matter) and therefore there are examples of interactions fitted to fission properties like Gogny-D1S [17,39], the old SkM* [40], or the more recent UNEDF1 [26,27] Skyrme parametrization.

Typical fission observables are the fission lifetimes, fragment mass distributions, and kinetic energy of the fragments. Fission barrier heights also are commonly considered as experimental "pseudodata." All those quantities are required in many physical scenarios such as the stability of superheavy elements or the final stages of the r process in stellar nucleosynthesis that are responsible for most of the abundance of heavy elements in the solar system. Fission remains a topic of high interest not only in several areas of basic science but also on the applications' side, where the issues of efficient energy production with nuclear reactors or the degradation of long-lived radioactive waste are of great interest [3,41].

It turns out that fission observables are quite sensitive to pairing correlations (see Ref. [38] for a recent discussion) owing to the strong dependence of the collective inertias on the inverse of the square of the pairing gap [42,43]. They are also very sensitive to the underlying theory used to describe collective motion [typically the adiabatic time-dependent HFB (ATDHFB) or the generator coordinate method (GCM)] and the approximations involved in the evaluation of the inertias (see Refs. [44–46] for different approximations). As a consequence, fission can be considered as a very demanding testing ground for theories and interactions used in nuclear structure calculations.

In the past decades there has been a renewed interest in microscopic fission studies [18–36,38] owing to the wealth of information in actinide nuclei [1], huge progress in the production of superheavy elements, via cold and hot fusion reactions, and new possibilities opened up by heavy-ion collisions with radioactive ion beams (see, for example, Refs. [47–55] and references therein). In particular, the theoretical description of fission in superheavy elements is quite relevant to better understand both the shell structure evolution and the appearance of new proton and/or neutron magic numbers in heavy nuclei [56,57]. Superheavy elements are also produced during the r process and their properties determine the upper end of the nucleosynthesis flow [58].

In addition, it should be kept in mind that, as a decay mode, spontaneous fission competes with α decay [59] and determines the stability of heavy and superheavy elements. It is therefore highly desirable to devote systematic microscopic studies, based on different effective EDFs, to the prediction of the spontaneous fission $t_{\rm SF}$ and α-decay t_α half-lives (see, for example, Refs. [25,29]). This is particularly relevant, taking into account the large uncertainties [38] associated with the different building blocks entering the Wentzel-Kramers-Brillouin (WKB) formula [60,61] used to computed the $t_{\rm SF}$ values.

Although the theoretical uncertainties in the determination of the absolute values of the fission observables are presumed to be large [38], the behavior of quantities as a function of mass number and/or along isotopic chains is reasonably well reproduced. Therefore, one expects to obtain a reasonable theoretical description of the physics of fission along isotopic chains extending up to the neutron drip line. Those regions are the territories where the fate of the nucleosynthesis of heavy nuclei is determined. To study the fission of neutron-rich nuclei, we have used a mean-field framework with the Gogny-EDF in the uranium isotopic chain up to the neutron drip-line nucleus ^{280}U. The three most relevant parametrizations of the Gogny-EDF [39], namely, D1S [17], D1N [62], and D1M [63], have been used in the calculations. The D1S parametrization is the oldest among the three and its fitting protocol included fission properties of ^{240}Pu. Along the years, D1S has built itself a strong reputation given its ability to reproduce a large collection of low-energy data all over the periodic table [17,18,23–25,39,64–81]. In particular, the parametrization D1S has already been successfully applied to the microscopic description of fission in heavy and superheavy nuclei (see, for example, Refs. [18,23,25] and references therein) and, for this reason, it is taken as a reference in the present study. However, D1S is not specially good in reproducing masses specially when moving away from the stability valley. To cure this deficiency the D1N parametrization was introduced. It provides a good fit to realistic neutron matter equation of state (EoS) and therefore it is expected to perform well in dealing with neutron-rich nuclei. However, this Gogny-EDF has scarcely been used and its performance in fission has to be validated. Finally, the D1M parametrization included in its fitting protocol not only realistic neutron matter EoS information but also the binding energies of all known nuclei. With an impressive rms for the binding energy of 0.798 MeV it represents an excellent and competitive choice to deal with nuclear masses. An extensive program to establish the merits and shortcomings of D1M in nuclear structure studies not only in even-even nuclei [62–65,82–86], but also in odd-A ones in the framework of the equal filling approximation (EFA) [82,84,85], is in progress. However, this parametrization has not been used systematically in fission studies before, and therefore its properties regarding fission have to be validated as in the case of D1N. As a consequence of these needs, we have decided to carry out calculations with the D1M parametrization for a selected set of nuclei consisting of $^{238-244}$Pu, $^{240-248}$Cm, ^{250,252}Cf, $^{250-256}$Fm, $^{252-256}$No, $^{256-260}$Rf, $^{258-262}$Sg, ^{264}Hs, and the $Z = 114$ nucleus ^{286}Fl, for which experimental data are available [87–91]. The comparison with these data and other quantities like fission barrier heights and excitation energies of fission isomers will be used to validate the results obtained with D1M. Later, calculations of fission properties for the uranium chain from ^{232}U up to the neutron drip line ^{280}U will be carried out. The comparison of the results obtained with

the three parametrizations will serve to give us an idea of the uncertainties associated with the Gogny-EDF used.

The paper is organized as follows. In Sec. II, we briefly outline the theoretical formalism used in the present work. The results of our calculations are discussed in Sec. III. First, in Sec. III A, we illustrate the methodology employed to compute the fission paths and other fission-related quantities in the case of ^{240}U. The same methodology has been used for all the nuclei studied in this paper. In Sec. III B, we discuss the D1M results for the nuclei $^{232-238}$U, $^{238-244}$Pu, $^{240-248}$Cm, ^{250,252}Cf, $^{250-256}$Fm, $^{252-256}$No, $^{256-260}$Rf, $^{258-262}$Sg, ^{264}Hs, and ^{286}Fl and compare them with available experimental data [87–91]. This section is mainly intended to validate D1M for fission studies. The systematics of the fission paths, spontaneous fission half-lives, and fragment mass in the isotopes $^{232-280}$U is presented in Sec. III C. We compare the results obtained with the D1S, D1N, and D1M parametrizations to demonstrate the robustness of the predicted trends in $^{232-280}$U with respect to particular choices of parametrizations. One of the main advantages of all the considered Gogny-EDFs is that they provide a self-contained approach to pairing correlations [39]. Owing to the differences in the corresponding fitting protocols [17,62,63], each of the EDFs displays a different pairing content [65]. This, by itself, provides some insight into the impact of pairing correlations on fission properties in $^{232-280}$U. However, in Sec. III D, we explicitly discuss the impact of pairing correlations on the predicted t_{SF} values for $^{232-280}$U by increasing artificially the pairing strengths by 5% and 10%, respectively. Finally, Sec. IV is devoted to the concluding remarks and work perspectives.

II. THEORETICAL FRAMEWORK

The mean-field approximation [6] based on wave functions $|\Phi_{\rm HFB}\rangle$ of the HFB type has been used in the present study. Constraints in the mean value of the axially symmetric quadrupole $\hat{Q}_{20}$, octupole $\hat{Q}_{30}$, and the necking $\hat{Q}_{\rm Neck}(z_0, C_0)$ operators have been used. The last constraint, as discussed in Sec. III A, allows us to reach two-fragment (2F) solutions starting from the one-fragment (1F) ones [23,24,38]. As a consequence of the axial symmetry imposed on our HFB wave functions $|\Phi_{\rm HFB}\rangle$, the mean values of the multipole operators $\hat{Q}_{\mu\nu}$ with $\nu \neq 0$ are zero by construction. Aside from the constraints already mentioned, as well as the usual ones on both the proton and the neutron numbers, a constraint on the operator $\hat{Q}_{10}$ is used to prevent spurious effects associated with the center-of-mass motion.

The HFB quasiparticle operators [6] have been expanded in an axially symmetric (deformed) harmonic oscillator (HO) basis containing states with J_z quantum numbers up to 35/2 and up to 26 quanta in the z direction. The basis quantum numbers are restricted by the condition

$$2n_\perp + |m| + \frac{1}{q} n_z \leqslant M_{z,\rm MAX}, \tag{1}$$

with $M_{z,\rm MAX} = 17$ and $q = 1.5$. This choice is well suited for the elongated prolate shapes typical of the fission process [23,38]. For each of the considered nuclei and each of the constrained configurations $(Q_{20}, Q_{30}, Q_{\rm Neck}, \dots)$ the two lengths b_z and $b_\perp$ characterizing the HO basis have been optimized so as to minimize the total HFB energy. With the choice of basis size and the minimization of the energy with the oscillator lengths, the relative energies determining the dynamics of the fission process are well converged. For the solution of the HFB equations, an approximate second-order gradient method [92] has been used. The method is very robust and the typical number of iterations to converge is quite small (a few tens) as compared to other methods. In addition, the complexity in the handling of constraints does not increase with its number.

Concerning the different interaction terms, the two-body kinetic energy correction has been fully taken into account (including exchange and pairing channels) in the variational procedure. However, the Coulomb exchange term is considered in the Slater approximation [93], while the Coulomb and spin-orbit contributions to the pairing field have been neglected.

The spontaneous fission half-life is computed (in seconds) with the WKB formalism [42] as

$$t_{\rm SF} = 2.86 \times 10^{-21} \times (1 + e^{2S}), \tag{2}$$

where the action S along the quadrupole constrained fission path reads

$$S = \int_a^b dQ_{20} \sqrt{2B(Q_{20})[V(Q_{20}) - (E_{\rm GS} + E_0)]}. \tag{3}$$

Here the integration limits a and b are the classical turning points [42] below the barrier and corresponding to the energy $E_{\rm GS} + E_0$. The potential $V(Q_{20})$ is given by the HFB energy corrected by the zero-point energies stemming from the restoration of the rotational symmetry $\Delta E_{\rm ROT}(Q_{20})$ and the fluctuations in the quadrupole moment $\Delta E_{\rm vib}(Q_{20})$. The rotational correction $\Delta E_{\rm ROT}(Q_{20})$ has been computed, in terms of the Yoccoz moment of inertia, according to the phenomenological prescription discussed in Refs. [66,67]. This correction plays a key role in determining the shape of the potential $V(Q_{20})$ because it can be as large as 6–7 MeV and its value is proportional to the degree of symmetry breaking, i.e., the value of the deformation Q_{20} [78].

Two methods have been used for the evaluation of the collective mass $B(Q_{20})$ and the vibrational energy correction $\Delta E_{\rm vib}(Q_{20})$. One is the cranking approximation [44–46] to the ATDHFB scheme [6]. In this case,

$$B_{\rm ATDHFB}(Q_{20}) = \frac{1}{2} \frac{\mathcal{M}_{-3}(Q_{20})}{\mathcal{M}_{-1}^2(Q_{20})}, \tag{4}$$

where the moments $\mathcal{M}_{-n}(Q_{20})$ of the generating quadrupole field read

$$\mathcal{M}_{-n}(Q_{20}) = \sum_{\mu\nu} \frac{|\hat{Q}^{20}_{\mu\nu}|^2}{(E_\mu + E_\nu)^n} \tag{5}$$

and $\hat{Q}^{20}_{\mu\nu}$ is the 20 component of the quadrupole operator in the quasiparticle representation [6]. The quasiparticle energies E_μ are the ones obtained in the solution of the HFB equations. The ATDHFB zero-point vibrational correction $\Delta E_{\rm vib}(Q_{20})$ is given by

$$\Delta E_{\rm vib,ATDHFB}(Q_{20}) = \tfrac{1}{2} G(Q_{20}) B^{-1}_{\rm ATDHFB}(Q_{20}), \tag{6}$$

where

$$G(Q_{20}) = \frac{1}{2}\frac{\mathcal{M}_{-2}(Q_{20})}{\mathcal{M}^2_{-1}(Q_{20})} \tag{7}$$

is the width of the overlap between two configurations with similar quadrupole moments.

The second method is based on the Gaussian overlap approximation (GOA) to the GCM [6]. Here, the collective mass reads

$$B_{\rm GCM}(Q_{20}) = \frac{1}{2}\frac{\mathcal{M}^2_{-2}(Q_{20})}{\mathcal{M}^3_{-1}(Q_{20})} \tag{8}$$

and $\Delta E_{\rm vib,GCM}(Q_{20})$ is given by Eq. (6) but replacing the ATDHFB mass with the GCM one. We have evaluated the spontaneous fission half-life $t_{\rm SF}$ [Eq. (2)] with the two schemes outlined above. The reason is that the ATDHFB masses are typically around 1.5 to 2 times larger than the GCM ones [38,61]. As a consequence, the action in the exponent defining $t_{\rm SF}$ is, in the ATDHFB case, between 20% and 40% larger than the GCM one. Depending on the value of the action, this increase can represent a difference of several orders of magnitude in the $t_{\rm SF}$ results. We also have to keep in mind that the inertias are computed in the so-called "perturbative cranking approximation" that is known to underestimate the real inertia values by a factor as small as 0.7, implying a reduction of a typical 15% in the action. For a thorough comparison of different forms of the collective inertia in the framework of Skyrme-like EDFs, including the ones in Eqs. (4) and (8), and including also the different computational schemes the reader is referred to Ref. [61].

In Eq. (3), the parameter E_0 accounts for the true ground-state energy once the zero-point quadrupole fluctuations are considered. Although it is not difficult to estimate its value using the curvature of the energy around the ground-state minimum and the values of the collective inertias [30], we have followed the usual recipe [23,38] of considering it as a free parameter that takes four different values (i.e., $E_0 = 0.5$, 1.0, 1.5, and 2.0 MeV). In this way we can estimate its impact on the predicted spontaneous fission half-lives.

To summarize the previous discussions, we conclude that the $t_{\rm SF}$ values obtained within our computational scheme are subject to several uncertainties related to the following items.

(i) *The characteristics of the different parametrizations of the Gogny-EDF considered.*

(ii) *The impact of triaxiality in the fission path.* It is well known that the configurations around the top of the inner barrier can reduce their energies when triaxiality is allowed. It is also possible in some superheavy nuclei that their oblate ground state evolves towards fission through a triaxial path. In our case, we have kept axial symmetry as a self-consistent symmetry along the whole fission path to reduce the already substantial computational effort. However, for a few selected configurations around the inner barrier we have allowed triaxiality to set in as to study the reduction of the inner barrier height. Typically, the lowering represents at most a few MeV when triaxial shapes are allowed [18,32]. However, the lowering of the inner barrier comes together with an increase of the collective inertia [31,94] that tends to compensate in the final value of the action. Therefore, the impact of triaxiality in the final value of $t_{\rm SF}$ is very limited and it has not been considered in the present study. In addition, previous studies [31] analyzing the *dynamical* path to fission have corroborated the insignificant role played by triaxiality to determine lifetimes.

(iii) *The value of the parameter E_0.* This is particularly relevant in the case of long-lived isotopes with wide and high fission barriers because the different E_0 values provide different classical turning points a and b [see Eq. (3)] and therefore modify in a substantial way the final value of the action integral.

(iv) *The assumptions involved in the computation of the collective masses as well as the zero-point corrections to the HFB energies.* Note that, for example, within the "perturbative cranking" scheme [44–46], only the zero-order approximation is used instead of the full linear-response matrix.

(v) *Pairing correlations.* They play a key role in the computation of both the zero-point energies associated with quantum fluctuations and the collective masses. In fact, as we see in Sec. III D (see also Ref. [38]), changes of 5% or 10% in the pairing strengths of the original Gogny-D1M EDF can modify the predicted $t_{\rm SF}$ values by several orders of magnitude.

As a consequence, the predicted $t_{\rm SF}$ values will have large theoretical error bars spanning several orders of magnitude, implying that their absolute values cannot be used with confidence. However, the experimental isotopic and/or isotonic trends are reproduced with much higher accuracy, giving us confidence on the validity of our predictions in that respect.

Finally, we have computed the α-decay half-lives using the parametrization [95]

$$\log_{10} t_\alpha = \frac{AZ + B}{\sqrt{\mathcal{Q}_\alpha}} + CZ + D \tag{9}$$

of the phenomenological Viola-Seaborg formula [59]. The $\mathcal{Q}_\alpha$ value (in MeV) is obtained from the calculated binding energies for uranium and thorium isotopes as

$$\mathcal{Q}_\alpha = E(Z,N) - E(Z-2,N-2) - E(2,2). \tag{10}$$

In Eqs. (9) and (10), Z and N represent the proton and neutron numbers of the parent nucleus. However, $E(2,2) = -28.295\,674$ MeV [96], while $A = 1.640\,62$, $B = -8.543\,99$, $C = -0.194\,30$, and $D = -33.9054$ [95].

III. DISCUSSION OF THE RESULTS

In this section, we discuss all the results obtained. First, in Sec. III A, we illustrate the methodology used to compute the fission observables in the case of ^{240}U. In Sec. III B, we discuss the Gogny-D1M results for a set of U, Pu, Cm, Cf, Fm, No, Rf, Sg, and Fl nuclei for which experimental data are available [87–91]. The aim of these calculations is to validate D1M as a reasonable parameter set for fission studies. The systematics, provided by the D1S, D1N, and

D1M Gogny-EDFs, for the fission paths t_{SF} and t_{α} values, as well as the fragment mass in the uranium chain $^{232-280}$U, is presented in Sec. III C. Finally, in Sec. III D, we explicitly discuss the impact of pairing correlations on the predicted t_{SF} values for $^{232-280}$U using a modified Gogny-D1M EDF in which the pairing interaction strengths are increased by 5% and 10%, respectively.

A. An illustrative example: The nucleus ^{240}U

In Fig. 1(a), the evolution of the energy as a function of the mass quadrupole moment for the nucleus ^{240}U as the system evolves from its ground state to very elongated shapes is shown. The results obtained with the D1S, D1N, and D1M parametrizations are depicted. The energies shown in the plot are the HFB energies plus the ones coming from the zero-point rotational motion $E_{\rm HFB} + \Delta E_{\rm ROT}$. The zero-point vibrational energies $\Delta E_{\rm vib}$ (not included in the plot) are always considered in the evaluation of the lifetimes. The curves labeled D1S(1F), D1N(1F), and D1M(1F), respectively, correspond to 1F solutions of the HFB equations. To obtain such 1F solutions, we have first carried out reflection-symmetric Q_{20}-constrained calculations. Subsequently, for each value of the quadrupole moment the octupole degree of freedom has been explored by constraining on a large value of Q_{30} and then releasing the constraint to reach the lowest energy solution. Note that constraints with higher multipolarities are not explicitly included in these calculations but, as it corresponds to a self-consistent calculation, the density profile (and therefore the mean value of the multipole moments) is determined as to minimize the energy. The only drawback of this procedure is that with our representation of the energy it is a mere projection of a multidimensional path. As a consequence, kinks and multiple branches are common in this type of representation (the 2F quasifusion solution is an example). To help interpret the multidimensional energy surface, the values of Q_{30} and Q_{40} (to be discussed below) are very helpful.

Coming back to the figure, the three Gogny-EDFs provide 1F curves with rather similar shapes. The ground state is located at $Q_{20} = 14$ b, while a first fission isomer appears at $Q_{20} = 42$ b. Using the energies $E_{\rm HFB} + \Delta E_{\rm ROT}$, we have obtained (without triaxiality) the inner barrier heights 9.90, 9.42, and 9.47 MeV with the D1S, D1N, and D1M parametrizations, respectively. Those values, for D1S and D1N, are in agreement with the values 20 and 18.4 MeV, respectively [62], of the surface energy coefficient in nuclear matter a_s. In a semiclassical picture of fission, the energy as a function of the driving coordinate (elongation) is the result of the competition between the increasing surface energy (governed by the a_s value) and the decreasing Coulomb repulsion, which is independent of the nuclear interaction. Unfortunately, the value of a_s is not available in the literature for D1M. The excitation energies of the first fission isomers are 2.66, 2.79, and 3.61 MeV for D1S, D1N, and D1M, respectively. This quantity is associated with shell effects and it is usually believed to be strongly correlated with pairing correlations. Another noticeable feature from Fig. 1(a) is the emergence of a second fission isomer around $Q_{20} = 86$ b with its associated third fission barrier. As discussed in Sec. III C, such second

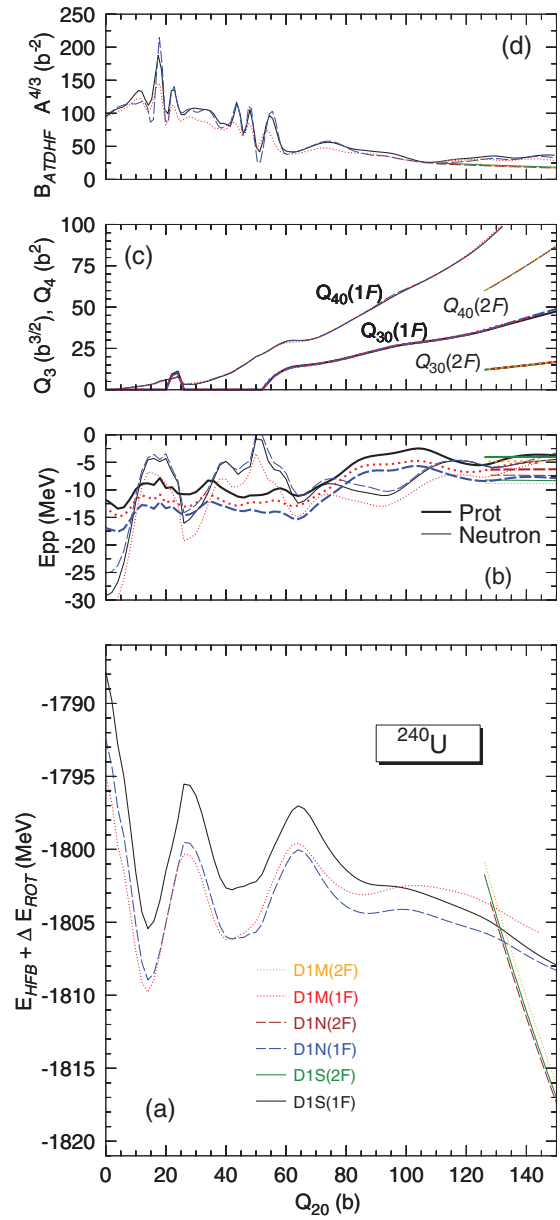

FIG. 1. (Color online) The HFB plus the zero-point rotational energies obtained with the D1S, D1N, and D1M EDFs are plotted in panel (a) as functions of the quadrupole moment Q_{20} for the nucleus ^{240}U. For each EDF, both the one-fragment (1F) and two-fragment (2F) solutions are included in the plot. The pairing interaction energies are depicted in panel (b) for protons (thick lines) and neutrons (thin lines). The octupole and hexadecapole moments corresponding to the 1F and 2F solutions are given in panel (c). The collective masses obtained within the ATDHFB approximation are plotted in panel (d). For more details, see the main text.

fission isomers are also found in the 1F curves of several uranium isotopes regardless of the Gogny-EDF employed [18]. Coming back to the second fission barrier, its height takes the values 8.41, 8.91, and 10.21 MeV, for D1S, D1N, and D1M, respectively. In this case, the trend observed in Ref. [71] relating the height of the second barrier with a_s (larger a_s leads to larger barrier heights) is not fulfilled. A possible

explanation is that at such large elongation the exchange properties of the interactions are more relevant than the surface properties. For the largest values of the quadrupole moment, the D1S and D1N curves show a similar decline owing to the decreasing of Coulomb repulsion. In this region the D1S curve is a couple of MeV lower in energy than D1N. This is not consistent with the behavior observed in Ref. [71] for D1 and D1S and attributed there to the a_s values of the two interactions. For D1, with an a_s coefficient 1.2 MeV larger than D1S, the HFB energy was around 10 MeV higher than for D1S. Finally, D1M shows a gentler decline than the ones provided by the D1N and D1S functionals. This points to a larger value of a_s than for D1N and D1S but the first barrier height values point in the opposite direction of a lower surface energy coefficient for D1M. These results do not follow the neat trend observed in Refs. [17,71] in the comparison between the D1 and D1S parametrizations. This problem deserves further study, although a possible explanation is that the properties of the region beyond the first barrier are driven by quantum effects (exchange and shell effects) rather than macroscopic properties like the surface energy coefficient a_s.

In Fig. 2, the 1F $E_{\rm HFB} + \Delta E_{\rm ROT}$ energies obtained in the axially symmetric calculations for the nucleus ^{240}U are compared with the ones obtained in the framework of triaxial calculations (see Ref. [65] for a thorough discussion of the framework and results with D1M). The curves depicted correspond to the D1M parametrization only, but similar results are obtained for the other parametrizations. The inclusion of the γ degree of freedom leads to the lowering of the energies in the $18\text{b} \leqslant Q_{20} \leqslant 32\text{b}$ range with $\gamma = 12^\circ$ being the largest value in the region. Compared with the axially symmetric one (i.e., 9.47 MeV) the height 7.51 MeV of the triaxial inner barrier in ^{240}U displays a reduction of 1.96 MeV.

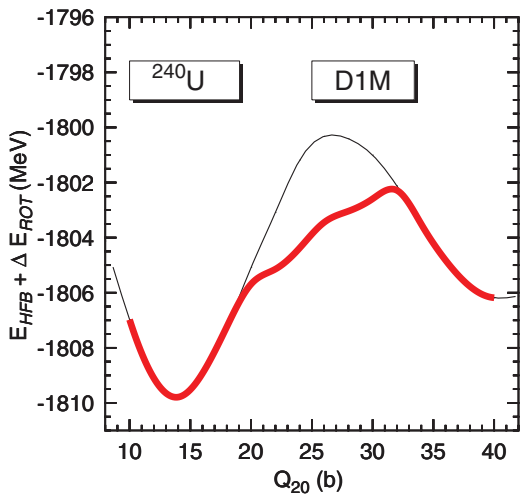

FIG. 2. (Color online) The HFB plus the zero-point rotational energies obtained in the framework of axially symmetric calculations (black thin curve), based on the Gogny-D1M EDF, for the nucleus ^{240}U are compared with the ones provided by triaxial calculations (red thick curve). Results are shown for configurations around the inner fission barrier (see Fig. 1).

Coming back to Fig. 1(a), very steep curves labeled D1S(2F), D1N(2F), and D1M(2F) are depicted. They correspond to solutions with two well-separated fragments and their energy corresponds to the quasifusion channel for the corresponding fragments. These 2F solutions can be reached, starting from the 1F ones, by constraining the hexadecapole moment $\hat{Q}_{40}$ [17,24]. Alternatively, one can resort to a constraint in the mean value of the necking operator $\hat{Q}_{\rm Neck}(z_0, C_0)$ [23,38]. For the nucleus ^{240}U, the 2F curves seem to intersect the 1F ones around $Q_{20} = 130$ b and exhibit a quasilinear decrease in energy for increasing values of the quadrupole moment [38]. The intersection of the 1F and 2F curves appears as a consequence of projecting multidimensional paths into a one-dimensional plot. Actually, there is a minimum action path with a ridge connecting the 1F and 2F curves in the collective space. As the determination of this path is quite cumbersome and its contribution to the action Eq. (3) is small, we have neglected its contribution to the action. Within this approximation we take the 2F curves, for which the charge and mass of the fragments lead to the minimum energy, as really intersecting the 1F ones. In practice, we have obtained the 2F curves by constraining the number of particles in the neck of the parent nucleus to a small value and then releasing the constraint in a self-consistent HFB calculation. To asses the stability of the procedure a set of calculations with different values of the neck parameters z_0 and C_0 [38] is performed to make sure that the same minimum is always reached. The steep decrease in the energy of the 2F solutions is a consequence of the direct relationship that exists in this case between Q_{20} and the fragments' separation distance R. As the quadrupole moment of a 2F solution increases, the shape of the fragments remains more or less the same but the distance R between them increases, decreasing the Coulomb repulsion between fragments and leading to the observed decrease of the energy [17,97].

The proton and neutron pairing interaction energies $E_{pp} = -1/2\text{Tr}\,(\Delta\kappa^*)$, are shown in Fig. 1(b). In the three cases, they follow the same trend as functions of the quadrupole moment, being smaller for neutrons (protons) with the D1M (D1N) parametrization. In all cases, the neutron pairing energies display minima at $Q_{20} = 0$ b around the top of the inner and second fission barriers as well as around the second fission isomer. However, E_{pp} exhibits maxima around $Q_{20} = 18$ and 50 b, respectively.

The octupole and hexadecapole moments are depicted, as functions of Q_{20}, in Fig. 1(c). The values obtained with the three Gogny-EDFs can hardly be distinguished from each other. However, it is also apparent from the figure that the moments corresponding to the 1F [i.e., Q_{30}(1F) and Q_{40}(1F)] and 2F [i.e., Q_{30}(2F) and Q_{40}(2F)] curves are quite different, reflecting the separation of the paths in the multidimensional space of parameters.

The collective masses $B_{\rm ATDHFB}$ are plotted in Fig. 1(d). Their evolution, as functions of Q_{20}, is well correlated with the one of the pairing interaction energies shown in Fig. 1(b). A similar pattern is found for the GCM masses (not shown in the plot), though their values are always smaller than the ATDHFB ones. For example, for $Q_{20} = 18$ b we have obtained the ratios $B_{\rm ATDHFB}/B_{\rm GCM} = 1.97,\ 1.98,$

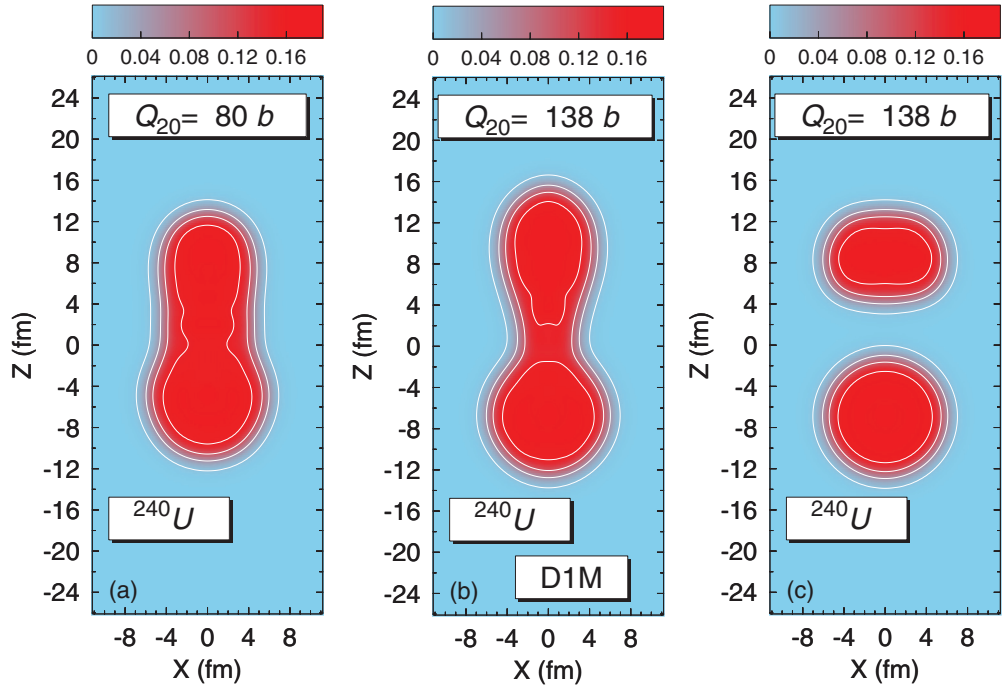

FIG. 3. (Color online) Density contour plots for the nucleus ^{240}U at the quadrupole deformations $Q_{20} = 80$ b [panel (a)] and $Q_{20} = 138$ b [panels (b) and (c)]. The density profiles in panels (a) and (b) correspond to 1F configurations, while the one in panel (c) represents a 2F solution. Results are shown for the parametrization D1M of the Gogny-EDF. Densities are in units of fm^{-3} and contour lines at drawn at 0.01, 0.05, 0.10, and 0.15 fm^{-3}.

and 1.85 for the D1S, D1N, and D1M parametrizations, respectively.

With all the previous ingredients at hand, we have computed the spontaneous fission half-lives using Eq. (2). Because we take the 1F and 2F curves as intersecting ones and do not include the effect of triaxiality on the inner barriers, our t_{SF} values should be regarded as lower bounds [38] to the real values. For the nucleus ^{240}U, we have obtained ($E_0 = 1.0$ MeV) $t_{SF} = 2.612 \times 10^{27}$ s, 2.161×10^{35} s, and 3.215×10^{42} s in the framework of the ATDHFB scheme for the D1S, D1N, and D1M parametrizations, respectively. The large differences in the predicted fission half-lives can be attributed to the differences in the fission paths and ATDHFB masses provided by the considered EDFs. To disentangle the different contributions, we have taken the D1S fission path and the D1N (D1M) ATDHFB mass to obtain 6.1×10^{26} s (1.5×10^{24} s) instead of the nominal value 2.612×10^{27} s. We conclude that the main effect is to be attributed to the different fission paths. The impact of the wiggles in the masses has also been estimated by replacing the mass with a smoothed-out mass (using a three-point filter) and the half-life changes with a factor 1.2, which is irrelevant in the present context. Using the GCM inertias, we obtain (again, $E_0 = 1.0$ MeV) smaller values $t_{SF} = 4.089 \times 10^{20}$, 3.764×10^{26}, and 3.552×10^{32} s. Larger ATDHFB t_{SF} values as compared with the GCM ones is, as discussed in Sec. III C, a general trend for all the studied uranium isotopes regardless of the particular functional employed. We thus see how the differences in the ATDHFB and GCM masses can have a strong impact on our predictions for fission observables. This is the reason why, for each Gogny-EDF, both kinds of collective masses have been considered in the computation of the spontaneous fission half-lives. However, increasing E_0 leads to smaller t_{SF} values in either the ATDHFB or the GCM frameworks (see below for a more quantitative assessment of the effect).

Finally, the density contour plots corresponding to the nucleus ^{240}U at the quadrupole deformations $Q_{20} = 80$ and 138 b are shown in Figs. 3(a), 3(b), and 3(c). Results are shown only for the Gogny-D1M EDF but similar ones have been obtained for the other parametrizations. For $Q_{20} = 138$ b two plots are presented corresponding to 1F and 2F solutions, respectively. The 2F solution in Fig. 3(c) consists of a spherical ^{132}Sn fragment plus an oblate and slightly octupole deformed ^{108}Mo fragment with $\beta_2 = -0.22$ and $\beta_3 = 0.03$ (referred to the fragment's center of mass). As we see in Sec. III C, oblate deformed fragments also appear as a result of fissioning other uranium isotopes. Similar results have been obtained in a recent study [38] based on the BCPM-EDF [37]. They deserve further analysis, as it is usually assumed [12,13] that fission fragments only exhibit prolate deformations. In our calculations, the deformed oblate fragment acquires this shape to minimize a large Coulomb repulsion of 195.19 MeV. The 2F solution shown is the one that minimizes the energy with the given quadrupole constraint. This does not necessarily mean that this is the configuration obtained after scission. In fact, it is observed experimentally that the mass number of the heavy fragment is close to 140 instead of the ^{132}Sn obtained as the minimum energy solution. Successful theories of scission [98]

postulate that the breaking of the nucleus takes place when the neck between fragments reaches some critical value. If we consider the rupture point as the position where the neck reaches its smallest width, we obtain for the heavy fragment the values $Z = 51.9$ and $N = 84.5$, which are close to $Z = 50$ and $N = 82$ of ^{132}Sn but lead to a mass of 136.4, which is closer to the experimental value. It has to be stressed that the values obtained should be taken as an approximation to the peaks of the mass distribution of the fragments. Obviously, to reproduce the broad mass fragment distribution observed experimentally, a dynamical theory considering the quantum mechanic evolution like, for instance, the one of Ref. [99] is required.

B. Heavy nuclei with known experimental data

In this section, the results obtained with the Gogny-D1M EDF for the set of nuclei $^{232–238}$U, $^{238–244}$Pu, $^{240–248}$Cm, ^{250,252}Cf, $^{250–256}$Fm, $^{252–256}$No, $^{256–260}$Rf, $^{258–262}$Sg, ^{264}Hs, and ^{286}Fl are discussed. The selected nuclei correspond to those where experimental data are available [87–89]. Previous theoretical results, based on the parametrization D1S, have already been presented in Refs. [18,23,25].

In Table I, we compare the predicted heights for the inner $B_{\rm I}^{\rm th}$ and outer $B_{\rm II}^{\rm th}$ barriers as well as the excitation energies $E_{\rm II}^{\rm th}$ of the fission isomers with the experimental ones $B_{\rm I}^{\rm exp}$, $B_{\rm II}^{\rm exp}$, and $E_{\rm II}^{\rm exp}$ [87,88]. The theoretical values have been obtained from the corresponding energies $E_{\rm HFB} + \Delta E_{\rm ROT}$ by looking at the energy differences between the ground-state energy and the energies of the corresponding maxima and minima. The axial $B_{\rm I}^{\rm th}$ values are larger than the experimental ones [87], reaching a maximal deviation $B_{\rm I}^{\rm th} - B_{\rm I}^{\rm exp} = 4.88$ MeV in ^{248}Cm. To explore the impact of the γ degree of freedom, for all the nuclei reported in Table I, we have performed triaxial calculations for configurations with $10b \leqslant Q_{20} \leqslant 40b$. The parameter γ takes on the values $0^\circ \leqslant \gamma \leqslant 12^\circ$ in this range of quadrupole deformations. As can be seen from panels (a) to (n) of Fig. 4 and the numerical values given in parentheses in the table, the triaxial inner barriers are systematically lower than the axial ones by up to 3.18 MeV in ^{248}Cm. They also display the position of the top of the barrier shifted to higher quadrupole deformations. The triaxial heights still overestimate the experimental ones. However, having in mind that the Gogny-D1M EDF has not been fine tuned to fission data and the large uncertainties in the extraction of the experimental inner barrier heights (a 1-MeV error bar is usually presumed), it is more important that the global trend observed in the experiment and other theoretical models (see, for example, Refs. [26,33,38] and references therein) is reasonably well reproduced. The D1M values for $B_{\rm I}^{\rm th}$ are consistent with the ones obtained in the framework of Gogny-D1S calculations [18].

In the case of the outer barriers, the inclusion of reflection-asymmetric shapes leads to a reduction of a few MeV. However, we still observe deviations of up to $B_{\rm II}^{\rm th} - B_{\rm II}^{\rm exp} = 4.75$ MeV with respect to the experimental data. As no significant effects are expected from triaxiality our results, as well as previous Gogny-D1S results [18], seem to indicate that other effects not related to the mass moments may be required to further decrease the predicted $B_{\rm II}^{\rm th}$ values. Whether it is the pairing degree of freedom or effects associated with symmetry restoration or the collective dynamics is something that remains to be explored. However, we have to keep in mind the model-dependent character of the experimental data for outer barriers heights that makes those quantities less reliable than the corresponding fission half-lives for a comparison with theoretical values. In the case of the fission isomer excitation energy, the largest difference observed $E_{\rm II}^{\rm th} - E_{\rm II}^{\rm exp}$=1.37 MeV occurs for ^{242}Pu.

TABLE I. The heights of the inner $B_{\rm I}^{\rm th}$ and second $B_{\rm II}^{\rm th}$ barriers as well as the excitation energies $E_{\rm II}^{\rm th}$ of the fission isomers, predicted with the Gogny-D1M EDF, are compared with the available experimental values $B_{\rm I}^{\rm exp}$, $B_{\rm II}^{\rm exp}$, and $E_{\rm II}^{\rm exp}$ [87,88]. The $B_{\rm I}^{\rm th}$ values obtained in the framework of triaxial calculations are given in parentheses. All the theoretical results have been obtained from the rotational corrected HFB energies. For more details, see the main text.

Nucleus	$B_{\rm I}^{\rm th}$	$B_{\rm I}^{\rm exp}$	$E_{\rm II}^{\rm th}$	$E_{\rm II}^{\rm exp}$	$B_{\rm II}^{\rm th}$	$B_{\rm II}^{\rm exp}$
^{234}U	7.60 (7.01)	4.80	3.32	–	8.09	5.50
^{236}U	8.33 (7.00)	5.00	3.17	2.75	8.69	5.67
^{238}U	9.06 (7.46)	6.30	3.37	2.55	9.54	5.50
^{238}Pu	8.77 (7.66)	5.60	3.20	2.40	7.75	5.10
^{240}Pu	9.45 (7.70)	6.05	3.36	2.80	8.57	5.15
^{242}Pu	9.90 (7.67)	5.85	3.57	2.20	9.18	5.05
^{244}Pu	10.16 (7.42)	5.70	3.83	–	9.60	4.85
^{240}Cm	8.98 (7.87)	–	2.55	2.00	6.13	–
^{242}Cm	9.78 (8.31)	6.65	2.77	1.90	6.99	5.00
^{244}Cm	10.38 (8.27)	6.18	3.02	2.20	7.70	5.10
^{246}Cm	10.75 (8.03)	6.00	3.29	–	8.13	4.80
^{248}Cm	10.68 (7.50)	5.80	3.32	–	8.28	4.80
^{250}Cf	11.38 (8.25)	–	2.81	–	7.09	3.80
^{252}Cf	10.96 (8.07)	–	1.37	–	6.79	3.50

In Fig. 5 we compare the Gogny-D1M $t_{\rm SF}$ values, obtained for the nuclei $^{232–238}$U, ^{240}Pu, ^{248}Cm, ^{250}Cf, $^{250–256}$Fm, $^{252–256}$No, $^{256–260}$Rf, $^{258–262}$Sg, ^{264}Hs, and ^{286}Fl within the GCM and ATDHFB schemes, with the experimental data [89]. Results are shown for $E_0 = 0.5$, 1.0, 1.5, and 2.0 MeV, respectively (see Sec. II). The effect of triaxiality has not been taken into account in the calculations. The experimental fission half-lives expand a range of 27 orders of magnitude. The

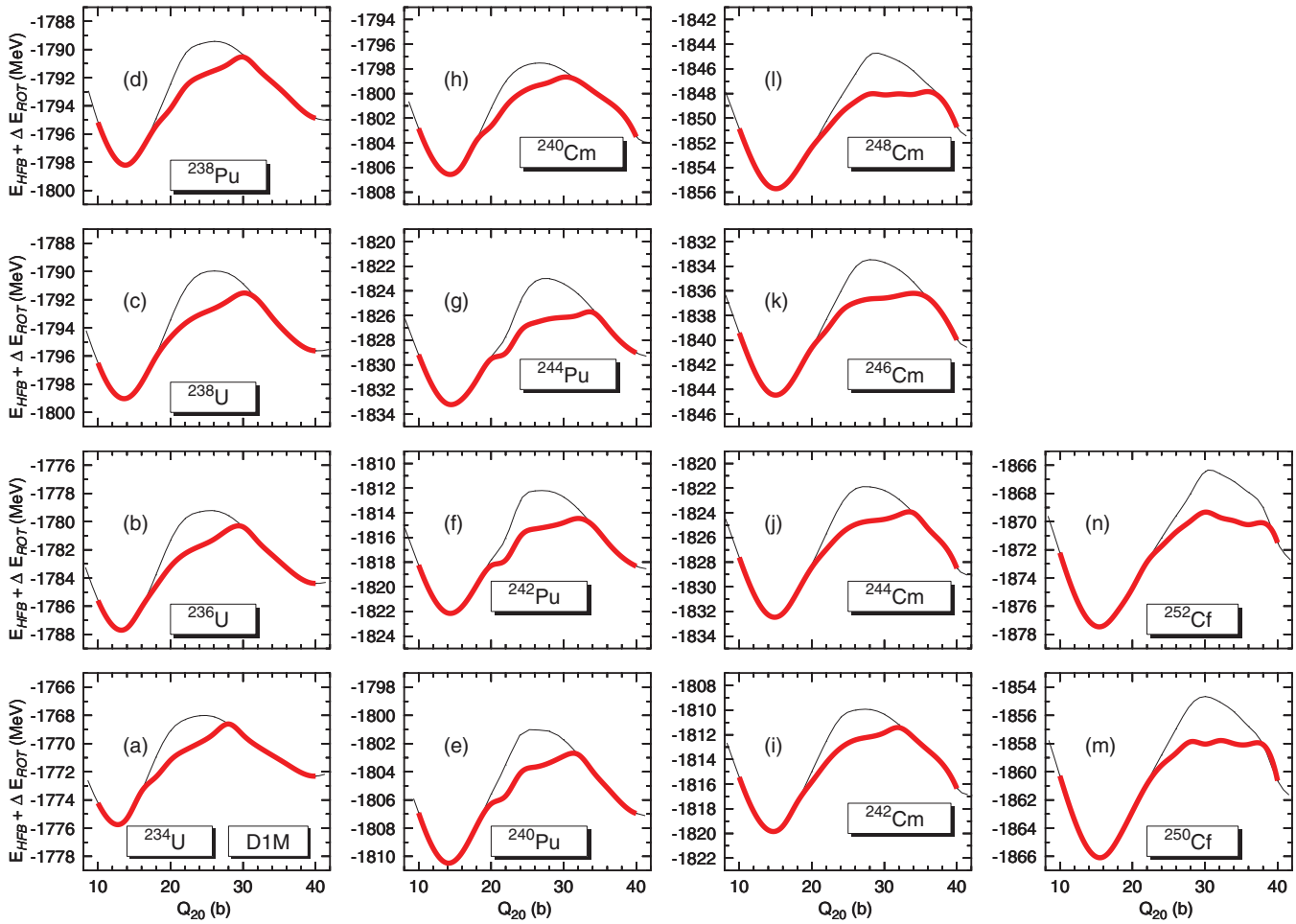

FIG. 4. (Color online) The HFB plus the zero-point rotational energies obtained in the framework of axially symmetric calculations (black thin curve), based on the Gogny-D1M EDF, for the nuclei $^{234–238}$U, $^{238–244}$Pu, $^{240–246}$Cm, and ^{250,252}Cf are compared with the ones provided by triaxial calculations (red thick curve). Results are shown for configurations around the inner fission barrier.

theoretical predictions display a larger variability depending on whether the GCM or ATDHFB scheme is used as well as on the E_0 parameter. For example, differences of up to 12, 9, 7, and 5 orders of magnitude occur in $^{232–238}$U, $^{238–244}$Pu, ^{248}Cm, and ^{250}Cf, for $E_0 = 0.5$ MeV. Such differences become smaller for the heavier Fm, No, Rf, Sg, Hs, and Fl nuclei. However, increasing E_0 leads to smaller t_{SF} in either of the two schemes. This reduction is particularly pronounced in the case of nuclei with higher and wider fission barriers. It is satisfying to observe that both the GCM and the ATDHFB Gogny-D1M schemes capture the large reduction of t_{SF} observed experimentally when going from ^{232}U to ^{286}Fl.

The comparison along isotopic chains reveals that the trend with neutron number is also reasonably well described. For the nuclei depicted in Fig. 5, both our Gogny-D1M and previous [23,25] Gogny-D1S calculations exhibit a similar trend as a function of the fissibility parameter Z^2/A. However, larger E_0 values are required in our case to improve the comparison with the experimental data. This is not surprising, as in most cases the Gogny-D1M 1F curves display a gentler decline for the largest deformations.

The proton (Z_1, Z_2), neutron (N_1, N_2), and mass (A_1, A_2) numbers of the 2F solution leading to the minimum energy for a given quadrupole moment and corresponding to the nuclei $^{238–244}$Pu, ^{248}Cm, ^{250,252}Cf, $^{250–256}$Fm, $^{252–256}$No, $^{256–260}$Rf, $^{258–262}$Sg, ^{264}Hs, and ^{286}Fl are shown in Fig. 6, as functions of the fissibility parameter Z^2/A of the parent nucleus. Fragment properties have been obtained from the 2F solutions and for the largest Q_{20} values available as to guarantee that those properties are nearly independent of the quadrupole moment (which is equivalent to the fragment's separation for 2F solutions) considered. In our calculations, the proton and neutron numbers in the fragments are mostly dominated by the $Z = 50$ and $N = 82$ magic numbers. Experimentally [90,91], the average masses $\overline{A}_H$ of the heavy fission fragments in $^{238–244}$Pu, ^{248}Cm, ^{250,252}Cf, and ^{254,256}Fm are nearly constant with a value around $\overline{A}_H = 140$ and deviations of 1 or 2 mass units. As mentioned before, the 2F solution discussed here is determined by the minimum energy requirement and according to several models of scission this is not necessarily the configuration obtained after the breakup of the parent nucleus. In the previous section, we briefly mentioned that if the breakup point is taken as the point where the well-developed

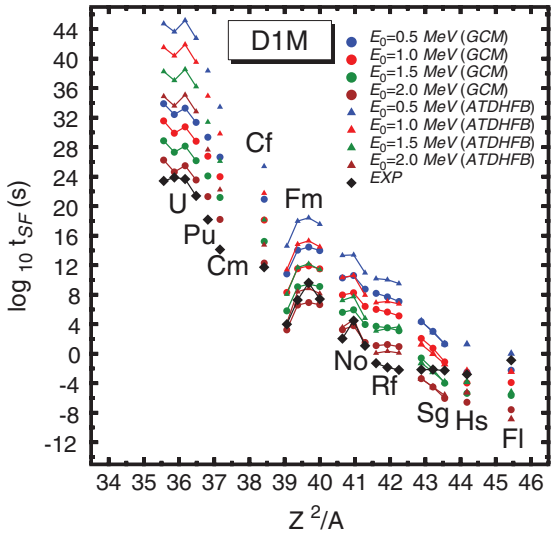

FIG. 5. (Color online) The spontaneous fission half-lives t_{SF} obtained for the nuclei $^{232-238}$U, ^{240}Pu, ^{248}Cm, ^{250}Cf, $^{250-256}$Fm, $^{252-256}$No, $^{256-260}$Rf, $^{258-262}$Sg, ^{264}Hs, and ^{286}Fl within the GCM and ATDHFB schemes are depicted as functions of the fissibility parameter Z^2/A and compared with the corresponding experimental data [89]. The theoretical results, based on the Gogny-D1M EDF, are shown for $E_0 = 0.5$, 1.0, 1.5, and 2.0 MeV, respectively. For more details, see the main text.

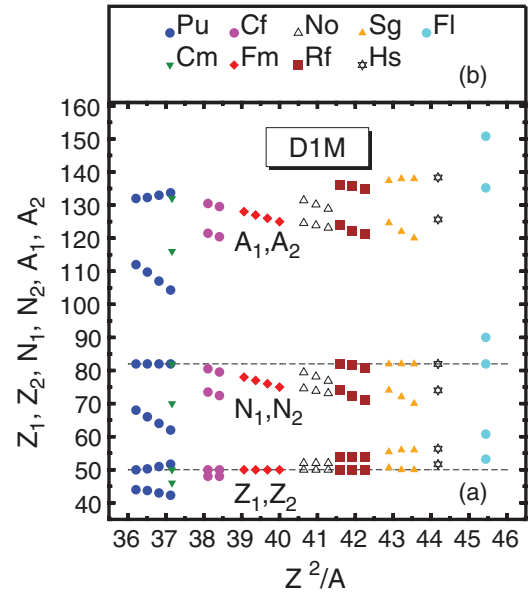

FIG. 6. (Color online) In panel (a), the proton (Z_1, Z_2), neutron (N_1, N_2), and mass (A_1, A_2) numbers of the two fragments resulting from the fission of $^{238-244}$Pu, ^{248}Cm, ^{250,252}Cf, $^{250-256}$Fm, $^{252-256}$No, $^{256-260}$Rf, $^{258-262}$Sg, ^{264}Hs, and ^{286}Fl [see panel (b)] are shown as functions of the fissibility parameter Z^2/A in the parent nucleus. Results have been obtained with the Gogny-D1M EDF. The magic proton $Z = 50$ and neutron $N = 82$ numbers are highlighted with dashed horizontal lines to guide the eye.

neck attains its minimum width, then the mass distribution becomes closer to the experimental values. However, a more microscopic model including quantum-mechanical effects like the one of Ref. [99] should be used for a sounder theoretical description. Because this kind of dynamical model is very involved computationally we do not dwell on this and we just keep in mind that the mass distribution of the two fragments leading to the minimum energy at the HFB level underestimates the mass of the heavier fragment by a few units. In addition to this general consideration, we can encounter locally examples where our model is not able to reproduce the delicate balance between macroscopic and shell effects that lead, for example, to mass asymmetric splittings in the heavy Fm isotopes. As an example, let us mention that a symmetric splitting is obtained in ^{256}Fm in disagreement with the rather large mass asymmetry $\overline{A}_L/\overline{A}_H = 112/141$ observed experimentally. Similar results have been obtained in previous calculations with the Gogny-D1S EDF [23]. However, the ratio $\overline{A}_L/\overline{A}_H = 124/136$ predicted for ^{260}Rf coincides with the one reported in Ref. [23].

To summarize the conclusions of this section, it has been shown that in spite of large theoretical uncertainties in the choice of the models to describe the relevant quantities, the Gogny-D1M [63] HFB framework provides a reasonable description of the tendencies with mass number of the physical observables. This validates the use of this parametrization to study the systematics of fission paths and other relevant quantities in the isotopes $^{232-280}$U that is presented in the next section. Results obtained with the D1S and D1N parameter sets are also discussed to quantify the typical uncertainties associated with the employed Gogny-EDF.

C. Systematics of fission paths, spontaneous fission half-lives, and fragment mass in uranium isotopes

In Figs. 7, 8, and 9 we have plotted the energies $E_{\rm HFB} + \Delta E_{\rm ROT}$, obtained with the D1S, D1N, and D1M Gogny-EDFs, for the nuclei $^{232-256}$U [panel (a)] and $^{258-280}$U [panel (b)]. Both the 1F (solid lines) and 2F (dashed lines) curves are shown in the plots. Starting from ^{232}U (^{258}U) in panel (a) [in panel (b)] all the curves have been successively shifted by 15 MeV to accommodate them in a single plot. Before commenting on more quantitative aspects of the results it is worth noticing that, regardless of the functional employed, the shapes of the 1F and 2F curves in $^{232-280}$U look rather similar, pointing to equivalent liquid-drop and shell-effect properties of the three EDFs considered.

As the neutron number increases, we observe a gradual decrease in the deformations corresponding to the absolute minima of the 1F curves in Figs. 7, 8, and 9 reaching the value $Q_{20} \approx 4$ b in the heavier isotopes. The nonzero Q_{20} value of the ground-state minimum in $^{270-280}$U is a direct consequence of the rotational energy correction that shifts spherical HFB minima to nonzero quadrupole moments, as it has already been documented in several regions of the nuclear chart [66,67,70,78]. If just the HFB energy is considered, these nuclei have a spherical intrinsic state consequence of neutron numbers close to $N = 184$ that is predicted to be a magic number in our calculations (see below).

An increase in the height of the inner fission barriers and the widening of the 1F curves is noticed in all the considered Gogny-EDFs as the two-neutron drip line is approached. As a

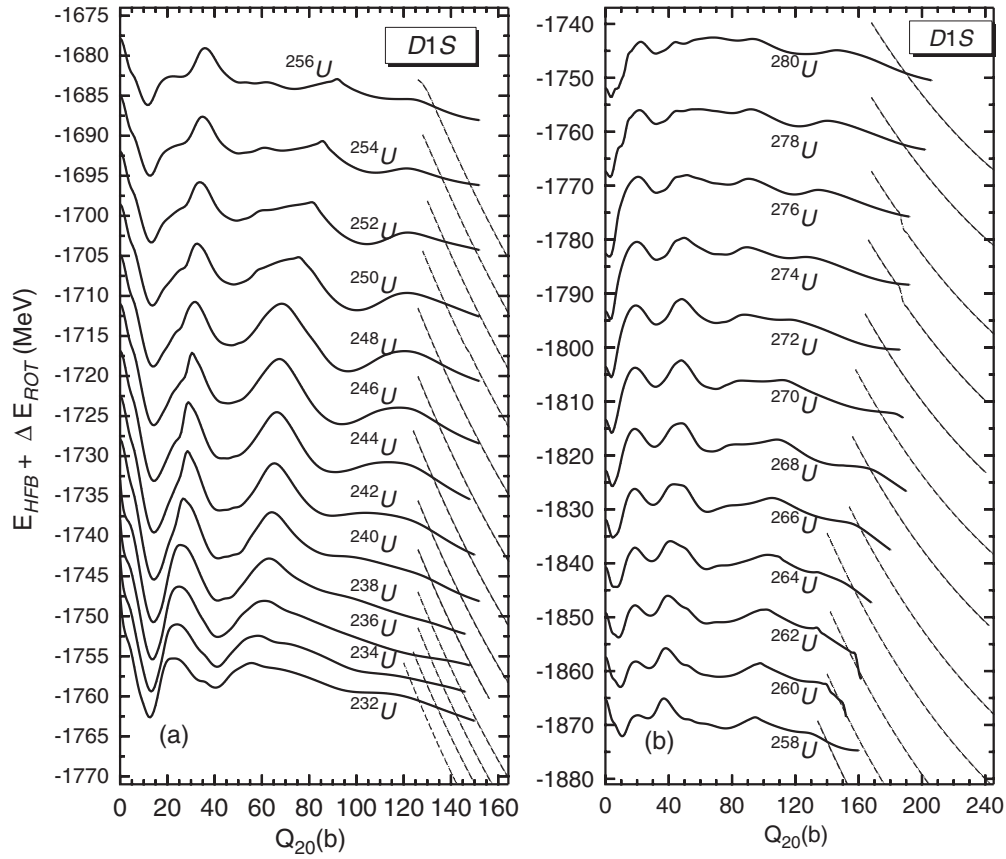

FIG. 7. The HFB plus the zero-point rotational energies obtained with the Gogny-D1S EDF are plotted in panel (a) for the nuclei $^{232–256}$U and in panel (b) for the nuclei $^{258–280}$U as functions of the quadrupole moment Q_{20}. Both the one-fragment (1F) and two-fragment (2F) solutions are shown in the plot with continuous and dashed lines, respectively. Starting from ^{232}U (^{258}U) in panel (a) [panel (b)] all the curves have been successively shifted by 15 MeV to accommodate them in a single plot. Note that the energy scales span different ranges in each panel. For more details, see the main text.

consequence, an increase in the spontaneous fission half-lives for the heavier uranium isotopes is expected. The existence of second fission isomers in several of the considered nuclei is also worth mentioning. For example, in $^{240–252}$U they exhibit quadrupole deformations $Q_{20} \approx 86$–96 b. The second fission isomers are also visible in the 1F curves of heavier isotopes, though in some cases the situation is not as well defined owing to the presence of several shallow minima. Similar results have been recently obtained with the BCPM-EDF [38].

To explore the role of the γ degree of freedom, we have performed Gogny-D1M triaxial calculations, for the isotopes $^{232–240,248,254,260,272–280}$U. The corresponding results for ^{240}U and $^{234–238}$U have already been shown in Figs. 2 and 4, respectively, but they are included again in Fig. 9 for the sake of completeness. For the heavier nuclei $^{248,254,260,272–280}$U, we have performed triaxial calculations for $4\text{b} \leqslant Q_{20} \leqslant 50\text{b}$, with $\gamma = 20^\circ$ being the largest value considered. The corresponding energies are shown in Fig. 9 and thin lines visible in the neighborhood of the first fission barrier.

To better understand the trends in binding energies for the uranium isotopes, the two-neutron separation energies (S_{2N}) are plotted in Fig. 10 for the three sets of calculations. We observe that whereas the D1N and D1M S_{2N} are rather similar, the D1S values are typically 1 MeV lower than the previous ones. These low values for D1S were reported in previous large-scale calculations [80] and show up as a systematic drift in the differences between the experimental and theoretical binding energies in heavy nuclei. In fact, the effort to correct this drift in the quest for an accurate mass table based on the Gogny-EDF led to the proposal of both D1N [62] and D1M [63]. Previous studies [62,63,65,82–85] suggest that, while improving the description of nuclear masses, both the D1N and the D1M sets still have the same essential predictive power to describe low-energy nuclear structure properties as the Gogny-D1S EDF. Nevertheless, more calculations are still required to substantiate this conclusion. The main features observed in the S_{2N} are the plateau between $N = 166$ and $N = 174$ and the sudden drop at $N = 186$ that signals the magic number character of $N = 184$.

In Fig. 11 the excitation energies of the first E_{I} fission isomers are plotted along with the first barrier height B_{I} in panel (a). In panel (b) the same quantities, but referred to the second isomeric well, are shown. The results for the three EDFs show a similar behavior with neutron number for the first barrier height B_{I}. A sudden drop is observed at $N = 164$ that is correlated with the plateau observed in the

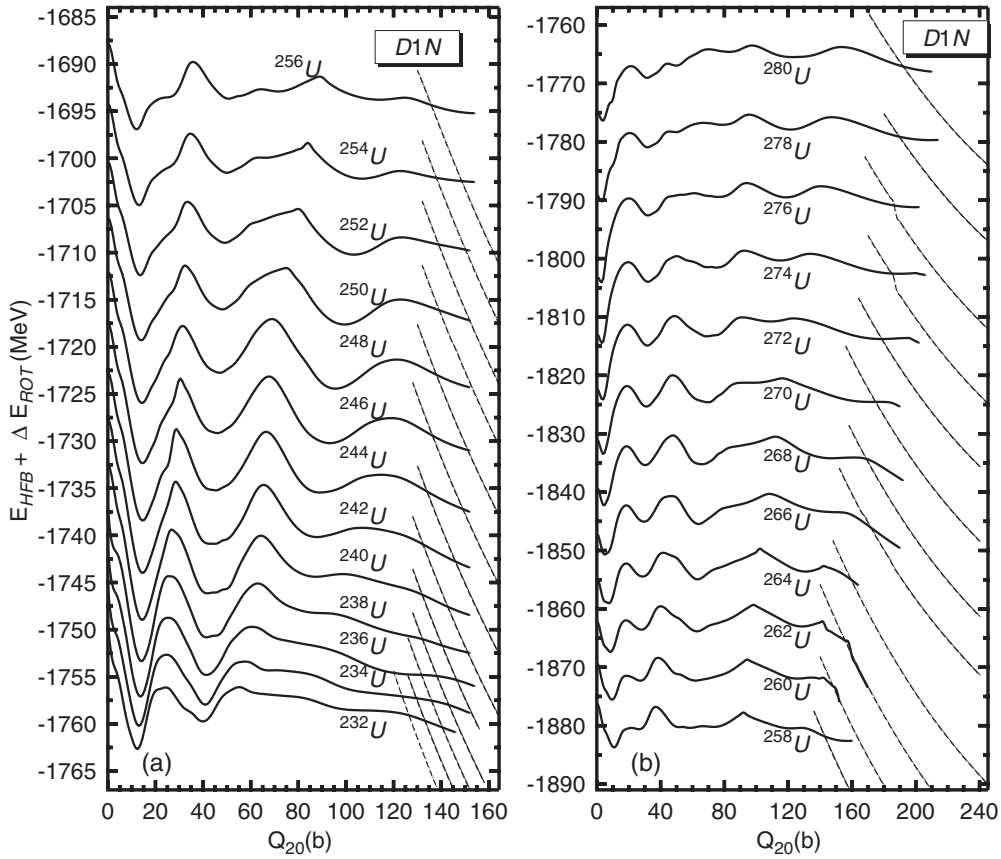

FIG. 8. The same as Fig. 7 but for the Gogny-D1N EDF.

S_{2N} plot. The excitation energies of the first fission isomer remain more or less constant with a value around 3 MeV up to $N = 164$, where they show a change of tendency and start to increase linearly with neutron number. At $N = 184$ there is a sudden drop accompanied by a drop in $B_{\rm I}$ characteristic of the filling of a new major shell. As previously mentioned, for D1M triaxial calculations in the neighborhood of the inner fission barriers have been carried out. Triaxiality reduces the B_I by 0.55, 0.59, 1.33, 1.60, and 1.96 MeV in the case of $^{232–240}$U, respectively. In spite of this reduction, the theoretical predictions still overestimate the experimental data [87,88] for $^{234–238}$U (see, also Table I). However, the axial barrier heights 8.30, 8.02, 8.44, 12.71, 13.32, 13.94, 11.42, and 9.54 MeV in the nuclei $^{248,254,260,272–280}$U are reduced by 2.70, 1.75, 0.56, 1.33, 0.86, 1.04, 1.01, and 0.88 MeV, respectively.

For the second isomeric well the behavior is more erratic and we can even observe the lack of second isomeric well in some nuclei. It is also worth noticing the similar predictions for $B_{\rm II}$ from the three EDFs and the large dispersion in the predicted $E_{\rm II}$ values.

With all the previous ingredients at hand, we have computed the spontaneous fission half-lives [Eq. (2)] for the considered uranium isotopes. The effect of triaxiality is not taken into account in the calculations. The $t_{\rm SF}$ values, predicted within the GCM and ATDHFB schemes, are plotted in Fig. 12 as a function of the neutron number. Results have been obtained with the Gogny-D1S [panel (a)], Gogny-D1N [panel (b)], and Gogny-D1M [panel (c)] EDFs. For each parametrization, we have carried out calculations with $E_0 = 0.5$, 1.0, 1.5, and 2.0 MeV, respectively. The experimental $t_{\rm SF}$ data for $^{232–238}$U are included in the plot.

The $t_{\rm SF}$ values predicted within the ATDHFB approximation are always larger than the GCM ones for a given E_0. For example, for $E_0 = 0.5$ MeV, differences of up to 12 orders of magnitude are obtained for the lighter isotopes. Such differences increase with increasing neutron number reaching 23, 31, and 26 orders of magnitude in the nucleus ^{276}U with the parametrizations D1S, D1N, and D1M, respectively. Increasing E_0 leads always to a decrease in $t_{\rm SF}$. It is satisfying to observe that all the parametrizations lead to the same trend in $t_{\rm SF}$, even though D1M provides the largest absolute values in half-lives and, as discussed in Sec. III B, larger E_0 values are required to improve the agreement with the available experimental data. This is a consequence of the shape of the 1F curves provided by the Gogny-D1M EDF for the considered uranium isotopes that are wider than for the other EDFs. Regardless of the EDF employed, we observe a steady increase in the spontaneous fission half-lives for neutron numbers $N \geqslant 166$, reaching a maximum at $N = 184$, which is predicted to be a magic neutron number in our calculations.

In Fig. 12, we have also plotted the α-decay half-lives computed with a parametrization [95] of the Viola-Seaborg formula [59] Eq. (9). To this end, we have used the binding energies obtained for the corresponding uranium and thorium

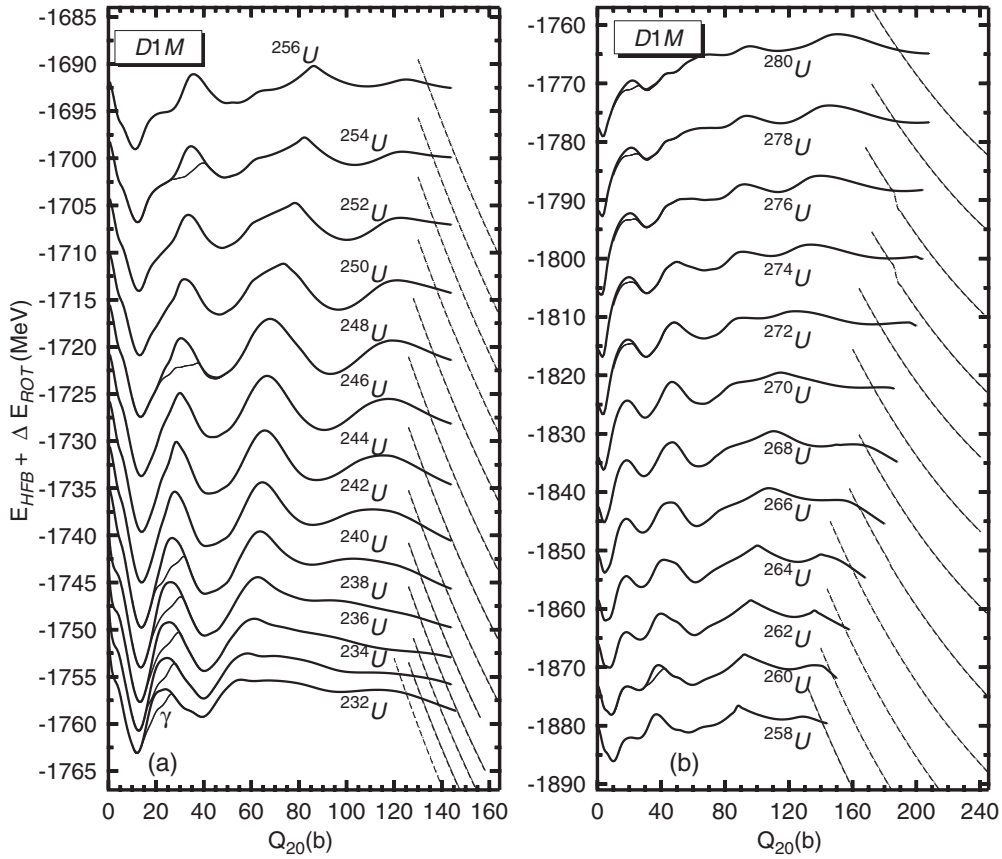

FIG. 9. The same as Fig. 7 but for the Gogny-D1M EDF. The energies obtained in the framework of triaxial calculations for the nuclei $^{232–240,248,254,260,272–280}$U (labeled as γ) are also included in the plot.

isotopes [see, Eq. (10)]. Here we stress that, at variance with the Gogny-D1S [17], both the D1N [62] and D1M [63] parametrizations have been tailored to give a better description of the nuclear masses and therefore their α-decay half-lives are expected to be much more realistic than the D1S ones. In all cases, a steady increase is observed in t_α as a function of the neutron number. Though the precise value depends on the selected EDF (i.e., $N = 144$ for D1S, $N = 150$ for D1N, and $N = 156$ for D1M), it is clearly seen that, for increasing neutron number, fission turns out to be faster than α decay.

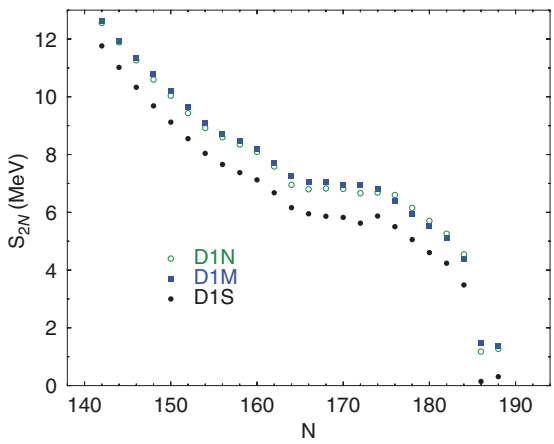

FIG. 10. (Color online) Two-neutron separation energies S_{2N} as a function of neutron number.

Our predictions compare well with the semiclassical results of Ref. [100] using the Extended Thomas-Fermi method for a Skyrme interaction. In that calculation very high barriers are predicted for $N = 184$ in the uranium isotopic chain contrary to some liquid-drop models. The barrier heights in those neutron-rich nuclei are correlated to the surface symmetry energy coefficient a_{ss}, an effect that deserves further study for the Gogny class of energy functionals.

The proton (Z_1, Z_2), neutron (N_1, N_2), and mass (A_1, A_2) numbers of the 2F solutions for $^{232–280}$U are shown in Fig. 13 as functions of the neutron number of the parent nucleus. Results have been obtained with the Gogny-D1S [panel (a)], Gogny-D1N [panel (b)], and Gogny-D1M [panel (c)] EDFs. Except for the nuclei $^{262–266}$ U, the neutron number in one of the fragments always corresponds to the magic number $N = 82$, while for the other fragment it increases as a function of the neutron number in the parent nucleus. The proton number in one of the fragments is always close to the magic one $Z = 50$ for $^{232–248}$U and $^{268–280}$U, which, in the case of the light isotopes, agrees well with the experiment [101]. It also varies almost linearly with the neutron number in the parent nucleus, except for $^{238–244}$U (it stabilizes at $Z = 50$) and ^{256}U (symmetric splitting). Note that a symmetric splitting is also predicted for the nuclei ^{262,264}U with the three EDFs. However, both the D1S and D1M parametrizations provide for ^{266}U a

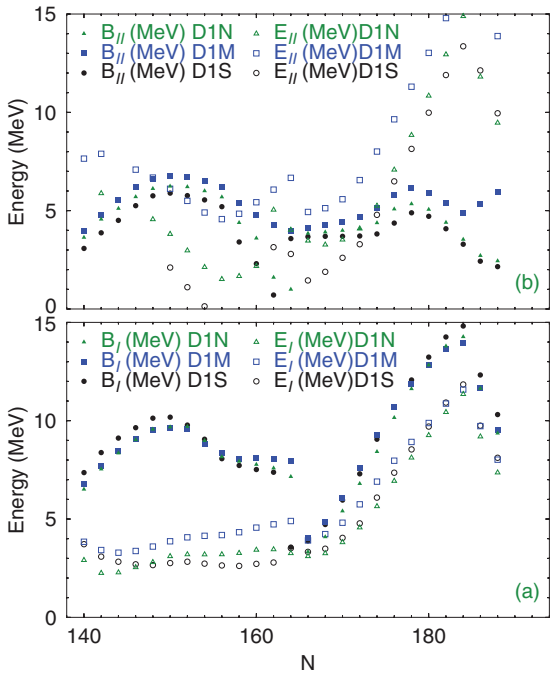

FIG. 11. (Color online) Excitation energies $E_{\rm I}$ ($E_{\rm II}$) and fission barrier heights $B_{\rm I}$ ($B_{\rm II}$) for the first (second) well are shown in panels (a) [(b)].

symmetric splitting while a small difference in the neutron and proton numbers of the two fragments is obtained with the Gogny-D1N EDF. The relevance of magic numbers in the fragment mass distribution is not surprising because it has been obtained by using a minimum of the energy criteria. Therefore, as discussed previously, they are not directly comparable to the real fission mass distribution.

We have also studied the evolution of the shapes in the fission fragments. A typical outcome of our calculations is shown in Fig. 14, where the density contour plots for the nuclei ^{234}U [panel (a)], ^{256}U [panel (b)], and ^{280}U [panel (c)] are plotted at quadrupole deformations ($Q_{20} = 150$, 150, and 220 b, respectively), corresponding to 2F solutions of the HFB equations (see Fig. 9). Results are shown for the parametrization D1M, but similar ones are obtained for the other Gogny-EDFs. The lighter (heavier) fragment in ^{234}U (^{280}U) is predicted to be oblate and slightly octupole deformed with $\beta_2 = -0.22$ and $\beta_3 = 0.02$. However, for the isotope ^{256}U we have obtained two identical fragments with $\beta_2 = -0.02$ and $\beta_3 = 0.01$. As already mentioned in Sec. III A, the appearance of oblate fragments in our calculations deserves further attention as fission fragments are usually assumed [12,13] to be prolate deformed.

The results discussed in this section, show that the same trends are obtained with the D1S, D1N, and D1M parametrizations. This gives us confidence in the robustness of our predictions with respect to the version of the Gogny-EDF employed. In particular, from the previous results and the ones discussed in Sec. III B, we conclude that the Gogny-D1M EDF represents a reasonable starting point to describe fission properties in the isotopes $^{232-280}$U and other heavy nuclei. With this in mind, we proceed to explicitly discuss the impact of pairing correlations in the next Sec. III D.

D. Varying pairing strengths in uranium isotopes

In this section, we discuss the impact of the strength of pairing correlations on the predicted spontaneous fission half-lives and other relevant fission properties in $^{232-280}$U.

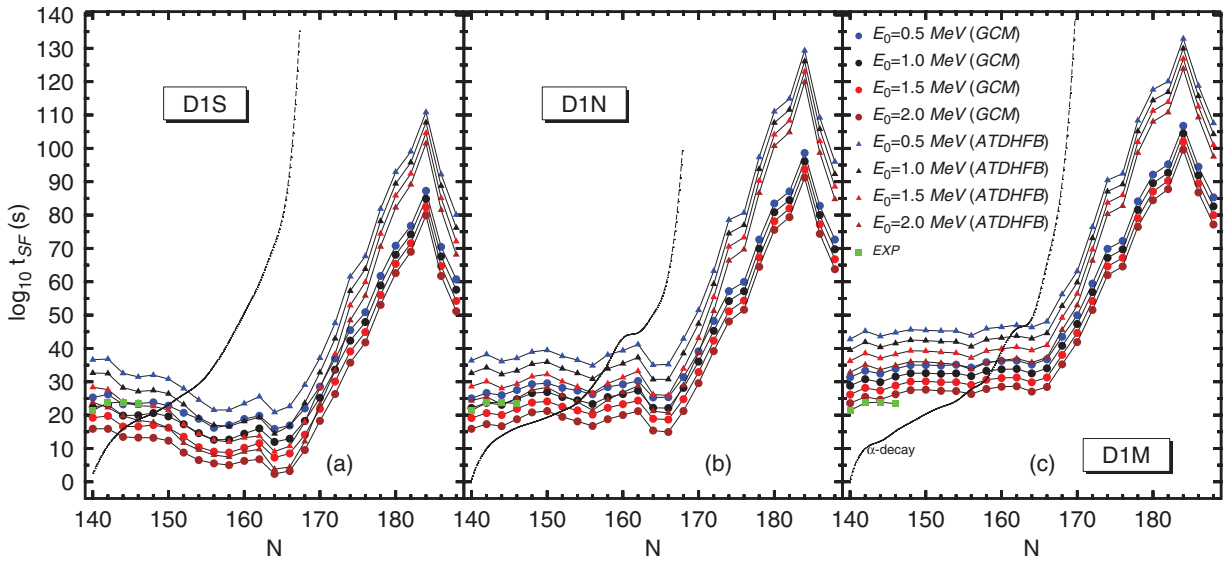

FIG. 12. (Color online) The spontaneous fission half-lives $t_{\rm SF}$, predicted within the GCM and ATDHFB schemes, for the isotopes $^{232-280}$U are depicted as functions of the neutron number. Results have been obtained with the Gogny-D1S [panel (a)], Gogny-D1N [panel (b)], and Gogny-D1M [panel (c)] EDFs. For each parametrization, calculations have been carried out with $E_0 = 0.5$, 1.0, 1.5, and 2.0 MeV, respectively. The experimental $t_{\rm SF}$ values for the nuclei $^{232-238}$U are included in the plot. In addition, α-decay half-lives are plotted with short-dashed lines. For more details, see the main text.

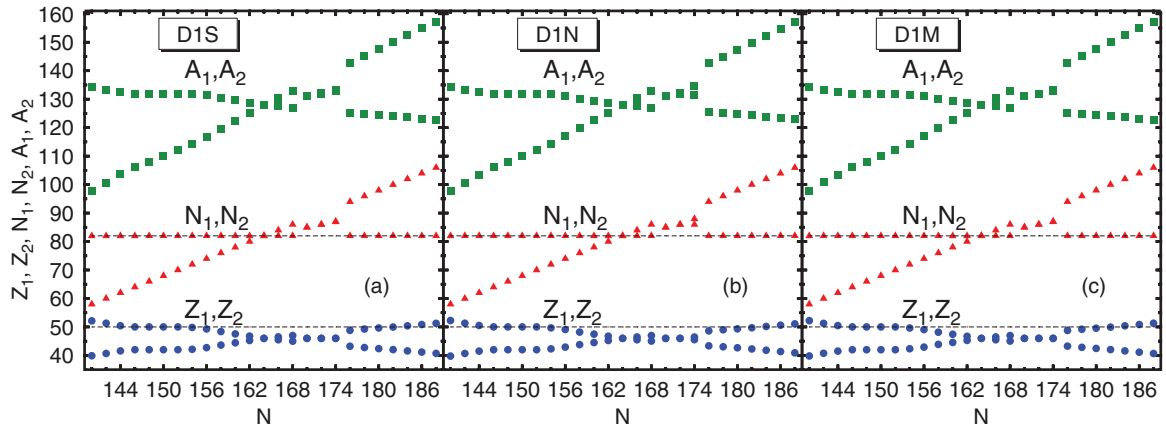

FIG. 13. (Color online) The proton (Z_1, Z_2), neutron (N_1, N_2), and mass (A_1, A_2) numbers of the two fragments resulting from the fission of the isotopes $^{232-280}$U are shown as functions of the neutron number in the parent nucleus. Results have been obtained with the Gogny-D1S [panel (a)], Gogny-D1N [panel (b)], and Gogny-D1M [panel (c)] EDFs. The magic proton $Z = 50$ and neutron $N = 82$ numbers are highlighted with dashed horizontal lines to guide the eye.

To this end, we have carried out self-consistent calculations with a modified Gogny-D1M EDF, in which a multiplicative factor η has been introduced in front of the HFB pairing field Δ_{kl} [6]. The corresponding pairing interaction energy reads

$$E_{pp}(\eta) = -\frac{\eta}{2}\mathrm{Tr}(\Delta\kappa^*). \tag{11}$$

For simplicity, we have considered the same η factor for both protons and neutrons. In addition to the normal Gogny-D1M EDF (i.e., $\eta = 1$), calculations have then been carried out with $\eta = 1.05$ and 1.10, respectively. Our main reason to consider different pairing strengths is that they are key ingredients in the computation of both the collective masses and the zero-point energies. For example, it has already been shown [42,43] that the collective mass is inversely proportional to some power of the pairing gap, i.e., the stronger the pairing correlations are the smaller the collective masses become. Similar η factors have been recently used in Ref. [38] as well as to describe pairing and rotational properties of actinides and superheavy nuclei in the framework of the RMF approximation (see, for example, Ref. [36] and references therein).

A typical outcome of our calculations is shown in Fig. 15(a), where we compare the three fission profiles obtained for

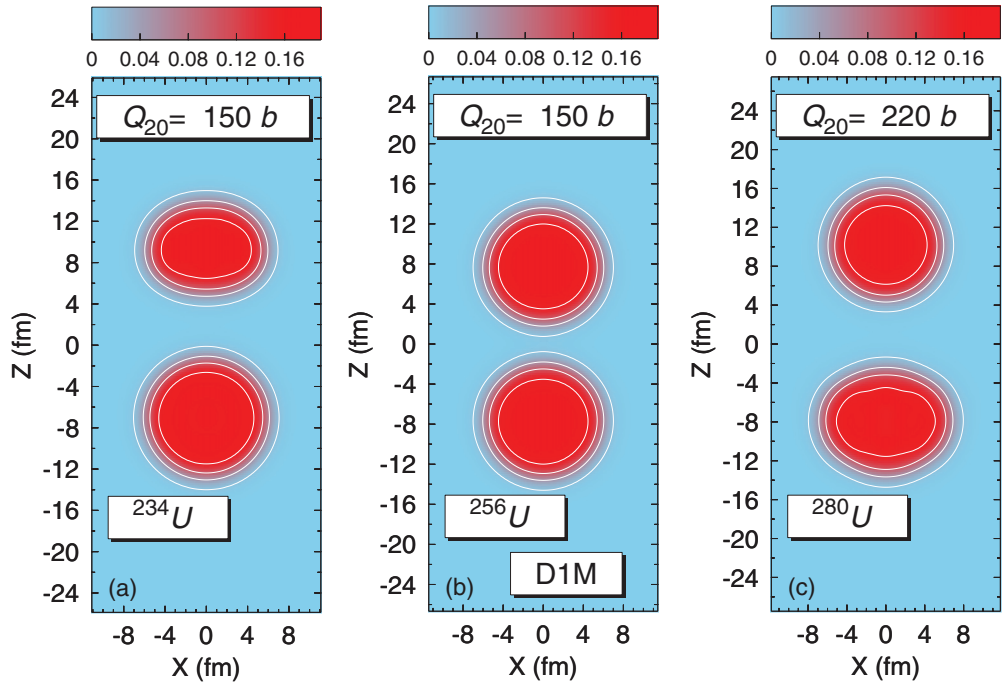

FIG. 14. (Color online) Density contour plots for the nuclei ^{234}U [panel (a)], ^{256}U [panel (b)], and ^{280}U [panel (c)]. The density profiles correspond to 2F solutions at the quadrupole deformations $Q_{20} = 150$, 150, and 220 b, respectively. Results are shown for the parametrization D1M of the Gogny-EDF. The density is in units of fm^3 and contour lines correspond to densities 0.01, 0.05, 0.10, and 0.15 fm^{-3}.

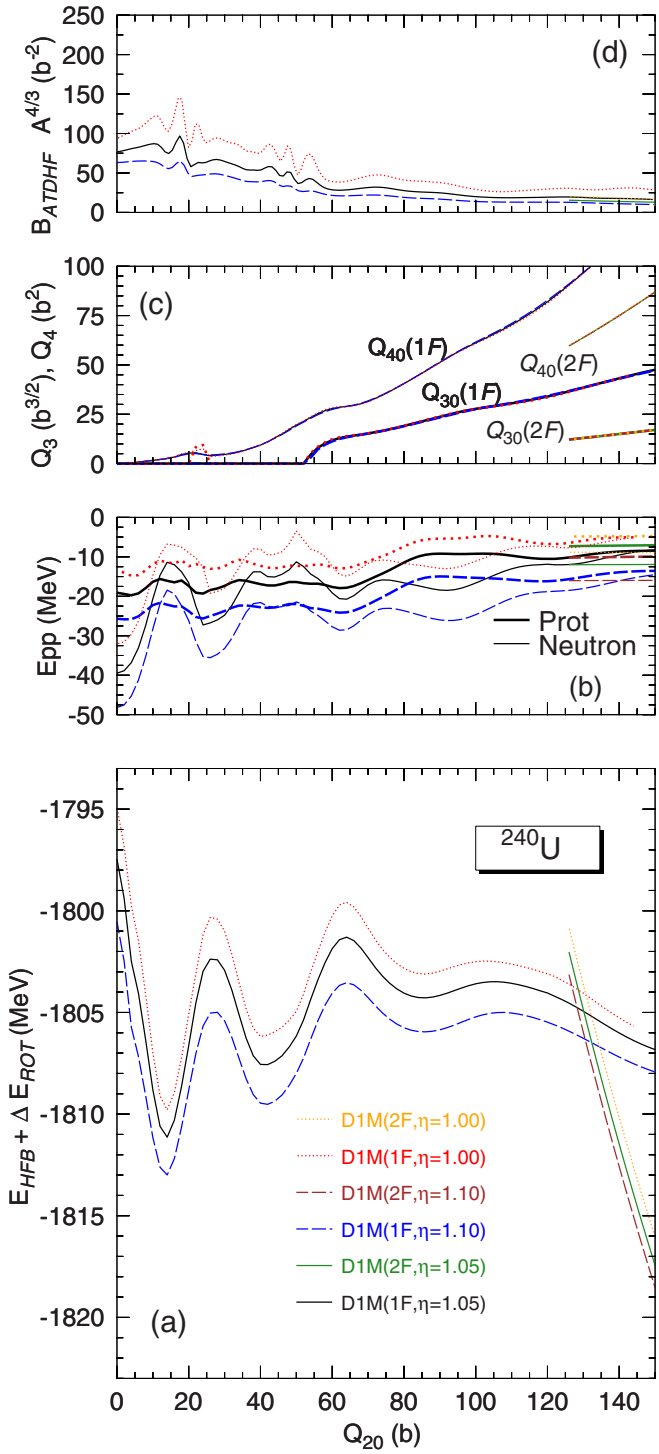

FIG. 15. (Color online) The HFB plus the zero-point rotational energies obtained with the normal ($\eta = 1.00$) and modified ($\eta = 1.05$ and 1.10) Gogny-D1M EDFs are plotted in panel (a) as functions of the quadrupole moment Q_{20} for the nucleus ^{240}U. For each η value, both the one-fragment (1F) and two-fragment (2F) solutions are included in the plot. The pairing interaction energies are depicted in panel (b) for protons (thick lines) and neutrons (thin lines). The octupole and hexadecapole moments corresponding to the 1F and 2F solutions are given in panel (c). The collective masses obtained within the ATDHFB approximation are plotted in panel (d). For more details, see the main text.

the nucleus ^{240}U using the normal ($\eta = 1.00$) and modified ($\eta = 1.05$ and 1.10) Gogny-D1M EDFs. For each η value, both the 1F and the 2F solutions are included in the plot. Except for the corresponding energy shifts, the 1F and 2F curves in ^{240}U and all the other uranium isotopes exhibit rather similar energy shapes. The ground state in ^{240}U located around $Q_{20} = 14$ b and its deformation decreases with increasing η. Increasing the pairing strength by 5% and 10%, we gain 1.11 and 2.29 MeV in binding energy, respectively. These quantities have to be compared to the HFB pairing correlation energy of 1.92 MeV obtained by subtracting the HFB energy to the Hartree-Fock one. We observe an increase of around 60% in correlation energy for $\eta = 1.05$, which is consistent with the exponential dependence of the correlation energy on the pairing strength. In spite of the large impact on correlation energies other quantities considered to fix the pairing strength like two neutron separation energies do not change significantly when η is increased justifying the range of η values considered. However, the heights of the inner barriers (8.76 MeV for $\eta = 1.05$ and 8.00 MeV for $\eta = 1.10$) display a reduction of 720 KeV and 1.47 MeV when compared to the one obtained using the normal Gogny-D1M EDF. The excitation energy of the first fission isomer, located at $Q_{20} = 42$ b, is lowered by 50 KeV ($\eta = 1.05$) and 140 KeV ($\eta = 1.10$).

The proton (dashed lines) and neutron (solid lines) pairing interaction energies are depicted in Fig. 15(b). They display similar trends as functions of the quadrupole moment though, as expected, they become larger with increasing η values. Concerning the multipole moments Q_{20}(1F), Q_{30}(1F), Q_{20}(2F), and Q_{30}(2F) shown in panel (c), one observes that they lie on top of each other, for all the considered η values.

In Fig. 15(d), the collective inertia B_{ATDHFB} is depicted. The behavior as a function of the quadrupole moment is similar in the three cases but the actual values are clearly correlated with the η factor. This is a direct consequence of the inverse dependence of the collective mass with the square of the pairing gap [42,43]. In particular, for $\eta = 1.05$ ($\eta = 1.10$) the ATDHFB mass is reduced, on the average, by 28% (46%). The GCM masses (not shown in the plot) are reduced by 28% and 35%, respectively. These reductions have a significant impact on the predicted fission half-lives. For example, for $E_0 = 1.0$ MeV we have obtained, within the ATDHFB scheme, $t_{\mathrm{SF}} = 3.215 \times 10^{42}, 3.051 \times 10^{31}$, and 2.575×10^{23} s for $\eta = 1.00$, $\eta = 1.05$, and $\eta = 1.10$, respectively.

In Fig. 16 we have plotted the spontaneous fission half-lives t_{SF}, predicted within the GCM and ATDHFB schemes, for the isotopes $^{232-280}$U as functions of the neutron number. Results have been obtained with the normal and modified Gogny-D1M EDFs. Calculations have been carried out with $E_0 = 0.5$ [panel (a)], 1.0 [panel (b)], 1.5 [panel (c)], and 2.0 MeV [panel (d)]. The experimental t_{SF} values for the nuclei $^{232-238}$U are included in the plot. In addition, α-decay half-lives are plotted with short-dashed lines.

On the one hand, the results shown in Fig. 16 illustrate the strong impact that pairing correlations have on the fission half-lives in the considered uranium isotopes. Increasing η leads to a reduction in both B_{ATDHFB} and B_{GCM}. As a consequence, for a given E_0, we observe a significant decrease in t_{SF} in either the ATDHFB or the GCM schemes. For example, for

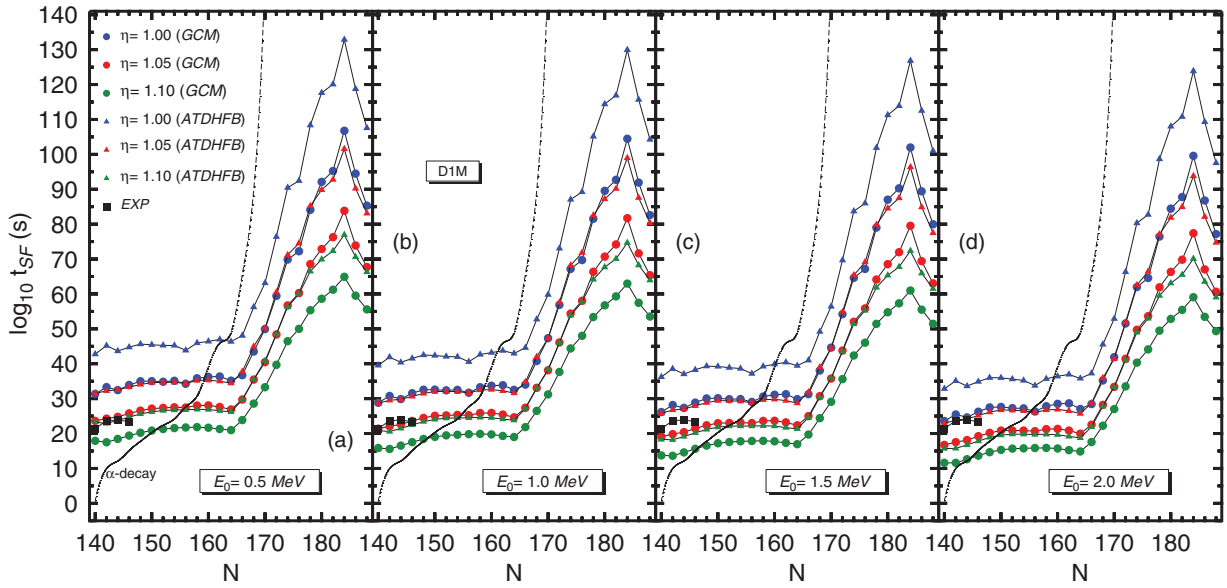

FIG. 16. (Color online) The spontaneous fission half-lives t_{SF}, predicted within the GCM and ATDHFB schemes, for the isotopes $^{232-280}$U are depicted as functions of the neutron number. Results have been obtained with the normal ($\eta = 1.00$) and modified ($\eta = 1.05$ and 1.10) Gogny-D1M EDFs. Calculations have been carried out with $E_0 = 0.5$ [panel (a)], 1.0 [panel (b)], 1.5 [panel (c)], and 2.0 MeV [panel (d)], respectively. The experimental t_{SF} values for the nuclei $^{232-238}$U are included in the plot. In addition, α-decay half-lives are plotted with short-dashed lines. For more details, see the main text.

$E_0 = 0.5$ MeV and within the GCM scheme, increasing the pairing strength by 5% (10%) leads to a reduction in t_{SF} of up to 9 (16) orders of magnitude in the light isotopes. Such a reduction becomes even more pronounced for the heavier isotopes, reaching 23 (42) orders of magnitude in the case of ^{276}U. Note that our results for $^{232-238}$U agree reasonably well with the experimental data. However, it is more important that, in spite of the large variability in the predicted t_{SF} values owing to pairing correlations, the same global features discussed in Sec. III C (see Fig. 12) still hold: (1) a steady increase in the spontaneous fission half-lives is observed for $N \geqslant 166$ reaching a maximum at $N = 184$; (2) beyond $N = 166$ the uranium isotopes can be considered stable with respect to spontaneous fission; (3) for increasing neutron number, fission turns out to be faster than α decay, with the transition point being around $N = 144$–150.

Once again, we stress that the results discussed in this section and Sec. III C point to the robustness of the overall trend predicted for the spontaneous fission half-lives in $^{232-280}$U using the more recent parametrizations of the Gogny-EDF. They suggest the use of experimental fission data, instead of the more traditional odd-even staggering, to fine tune the pairing strengths in those EDFs commonly employed in microscopic studies. They also point [38] to the relevance of beyond mean correlations associated with the interplay between pairing fluctuations and particle-number symmetry restoration [6] in the description of fission. Given the large uncertainties in the predicted t_{SF} values in our and other theoretical approaches with respect to pairing correlations and other building blocks affecting the WKB formula, it becomes obvious that a direct comparison with experiment is meaningless. Therefore, only the global trends, extracted from calculations performed under the same conditions along series of nuclei and/or isotopes, should be used to extract conclusions.

IV. CONCLUSIONS

In the present work, we have considered the evaluation of fission observables within the constrained HFB approximation based on Gogny-like EDFs. We have presented a detailed description of the methodology employed to obtain the fission paths in the studied nuclei. Besides the proton $\hat{Z}$ and neutron $\hat{N}$ number operators, we have considered constraints on the axially symmetric quadrupole $\hat{Q}_{20}$ and octupole $\hat{Q}_{30}$ and $\hat{Q}_{10}$ operators. In some instances, we have explored the role of the γ degree of freedom by means of triaxial calculations with simultaneous constraints on both the $\hat{Q}_{20}$ and the $\hat{Q}_{22}$ components of the quadrupole moment. However, HFB solutions corresponding to separated fragments have been reached with the help of the necking operator $\hat{Q}_{\rm Neck}(z_0, C_0)$. The 1F curves obtained in this way exhibit a rich topography including the ground state minimum, the inner and outer barriers as well as the first and second fission isomers. For larger deformations we have found 2F curves displaying a quasilinear decrease in energy for increasing values of the quadrupole moment. Zero-point quantum corrections have always been added to each of the mean-field solutions *a posteriori*. In particular, the rotational correction has been computed in terms of the Yoccoz moment of inertia, while two different schemes (i.e., the ATDHFB and GCM ones) have been employed in the calculation of both the collective inertia and the vibrational corrections. We have thoroughly discussed the uncertainties in the predicted spontaneous fission half-lives t_{SF} arising from different building blocks affecting the WKB formula.

We have carried out Gogny-D1M calculations for a selected set of actinides and superheavy elements. The comparison between the theoretical and experimental inner and second barrier heights as well as the excitation energies of fission isomers shows that the global trend observed in the experiment is reasonably well reproduced. The same is true in the case of the spontaneous fission half-lives, regardless of whether the ATDHFB or GCM masses are used. In particular, our results demonstrate that the Gogny-D1M HFB framework captures the severe experimental t_{SF} reduction between ^{232}U and ^{286}Fl as well as the trend along different isotopic chains. Another relevant source of information is the mass and charge of the resulting fission fragments, which are determined by the nuclear shape in the neighborhood of the scission point. In our calculations the proton and neutron numbers of the fragments are determined by energetic considerations and therefore they are mostly dominated by the $Z = 50$ and $N = 82$ magic numbers. Those values, however, underestimate by several mass units the experimental values pointing to the need of a better dynamical theory to describe postfission phenomena. The results obtained validate the D1M Gogny-EDF, originally tailored to better reproduce nuclear masses, for the study of fission properties in heavy and superheavy nuclei.

We have performed a systematic study of the fission properties in uranium nuclei, including very neutron-rich isotopes up to ^{280}U. To verify the robustness of our predictions, when extrapolated to very exotic N/Z ratios, calculations have been carried out with the three most recent incarnations of the Gogny-EDF, i.e., the parametrizations D1S, D1N, and D1M. The well-known underbinding of the heavier isotopes characteristic of the Gogny-D1S EDF is clearly visible in our calculations. Nevertheless, the fission paths still exhibit rather similar shapes regardless of the functional employed. An increase in the height of the inner fission barriers and the widening of the 1F curves appear as common features as we approach the two-neutron drip line. Second fission isomers are predicted for several uranium isotopes. From the systematics of the spontaneous fission half-lives, we conclude that, even when subject to large uncertainties, the Gogny HFB framework produces a trend which is quite robust. In particular, we have found that

(i) a steady increase in the spontaneous fission half-lives is observed for $N \geqslant 166$, with a peak at the neutron magic number $N = 184$;
(ii) beyond $N = 166$ the uranium isotopes can be considered stable with respect to spontaneous fission;
(iii) as a decay mode fission becomes faster than α emission for increasing neutron number.

In addition, the analysis of the masses and charges of the fission fragments reveals the key role played by the $Z = 50$ and $N = 82$ shell closures in the splitting of the considered uranium isotopes. Interesting enough, oblate deformed fragments are predicted in our calculations that deserve further attention because it is usually assumed that fission fragments exhibit prolate deformations.

In the present study special attention has been paid to the impact of pairing correlations on the fission properties in $^{232-280}$U. To this end, we have also considered a modified Gogny-D1M EDF in which the pairing strengths are increased by 5% and 10%, respectively. On the one hand, our calculations further corroborate the robustness of the predicted spontaneous fission half-life systematics. On the other hand, they also illustrate that modifications of such a small percent in the pairing strength can have a dramatic impact on the collective masses, therefore altering the absolute values of the fission half-lives by several orders of magnitude. Within this context, we advocate the use of experimental fission data, instead of the more traditional odd-even staggering, to fine tune the pairing strengths in those EDFs commonly employed in microscopic studies. Our results also point to the relevance of beyond mean correlations associated with the interplay between pairing fluctuations and particle number symmetry restoration in the description of nuclear fission.

Last but not least, let us also comment on a more methodological issue. Given the present state of affairs in the microscopic computation of spontaneous fission half-lives, even in the case of state-of-the-art approximations, it is highly desirable to explore new avenues in which the minimization of the action S [see Eq. (3)] acquires a central role. The first steps within the Skyrme-EDF framework have been undertaken very recently [102]. The action is proportional to the square root of the collective inertia and therefore any degree of freedom having an impact on it will play an essential role. In this respect, pairing correlations should be incorporated as an important degree of freedom, in addition to the more traditional quadrupole and octupole moments. Work along these lines is in progress and will be reported elsewhere.

ACKNOWLEDGMENTS

Work supported in part by MICINN Grants No. FPA2012-34694 and No. FIS2012-34479 and by the Consolider-Ingenio 2010 Program MULTIDARK CSD2009-00064. This work was completed while one of the authors (L.M.R.) participated at the INT13-3 program. The warm hospitality of the Institute for Nuclear Theory and the University of Washington is greatly acknowledged.

[1] H. J. Specht, Rev. Mod. Phys. **46**, 773 (1974).
[2] S. Björnholm and J. E. Lynn, Rev. Mod. Phys. **52**, 725 (1980).
[3] H. J. Krappe and K. Pomorski, in *Theory of Nuclear Fission*, Lectures Notes in Physics Vol. 838 (Springer, Berlin, 2012), p. 207.
[4] L. Meitner and O. R. Frisch, Nature (London) **143**, 239 (1939).
[5] N. Bohr and J. A. Wheeler, Phys. Rev. **56**, 426 (1939).
[6] P. Ring and P. Schuck, *The Nuclear Many-Body Problem* (Springer, Berlin, 1980).
[7] D. L. Hill and J. A. Wheeler, Phys. Rev. **89**, 1102 (1952).
[8] V. M. Strutinsky and H. C. Pauli, *Physics and Chemistry of Fission* (IAEA, Viena, 1969).

[9] V. M. Strutinsky, Nucl. Phys. A **95**, 420 (1967).
[10] V. M. Strutinsky, Nucl. Phys. A **122**, 1 (1968).
[11] W. D. Myers and W. J. Swiatecki, Nucl. Phys. A **81**, 1 (1966).
[12] P. Möller and A. Iwamoto, Phys. Rev. C **61**, 047602 (2000).
[13] P. Möller, D. G. Madlan, A. J. Sierk, and A. Iwamoto, Nature (London) **409**, 785 (2001).
[14] J. W. Negele, Nucl. Phys. A **502**, 371 (1989).
[15] J. Skalski, Phys. Rev. C **77**, 064610 (2008).
[16] M. Bender, P.-H. Heenen, and P.-G. Reinhard, Rev. Mod. Phys. **75**, 121 (2003).
[17] J. F. Berger, M. Girod, and D. Gogny, Nucl. Phys. A **428**, 23c (1984).
[18] J.-P. Delaroche, M. Girod, H. Goutte, and J. Libert, Nucl. Phys. A **771**, 103 (2006).
[19] V. Martin and L. M. Robledo, Int. J. Mod. Phys. E **18**, 788 (2009).
[20] N. Dubray, H. Goutte, and J.-P. Delaroche, Phys. Rev. C **77**, 014310 (2008).
[21] S. Pérez-Martín and L. M. Robledo, Int. J. Mod. Phys. E **18**, 861 (2009).
[22] W. Younes and D. Gogny, Phys. Rev. C **80**, 054313 (2009).
[23] M. Warda, J. L. Egido, L. M. Robledo, and K. Pomorski, Phys. Rev. C **66**, 014310 (2002).
[24] J. L. Egido and L. M. Robledo, Phys. Rev. Lett. **85**, 1198 (2000).
[25] M. Warda and J. L. Egido, Phys. Rev. C **86**, 014322 (2012).
[26] N. Nikolov, N. Schunck, W. Nazarewicz, M. Bender, and J. Pei, Phys. Rev. C **83**, 034305 (2011).
[27] J. McDonnell, N. Schunck, and W. Nazarewicz, *Proceedings of the 5th International Conference on "Fission and Properties of Neutron-Rich Nuclei" (ICFN5)* (Sanibel Island, 2012).
[28] J. D. McDonnell, W. Nazarewicz, and J. A. Sheikh, Phys. Rev. C **87**, 054327 (2013).
[29] J. Erler, K. Langanke, H. P. Loens, G. Martínez-Pinedo, and P.-G. Reinhard, Phys. Rev. C **85**, 025802 (2012).
[30] A. Staszczak, A. Baran, and W. Nazarewicz, Phys. Rev. C **87**, 024320 (2013).
[31] A. Baran, K. Pomorski, A. Lukasiak, and A. Sobiczewski, Nucl. Phys. A **361**, 83 (1981).
[32] H. Abusara, A. V. Afanasjev, and P. Ring, Phys. Rev. C **82**, 044303 (2010).
[33] H. Abusara, A. V. Afanasjev, and P. Ring, Phys. Rev. C **85**, 024314 (2012).
[34] B.-N. Lu, E.-G. Zhao, and S.-G. Zhou, Phys. Rev. C **85**, 011301 (2012).
[35] S. Karatzikos, A. V. Afanasjev, G. A. Lalazissis, and P. Ring, Phys. Lett. B **689**, 72 (2010).
[36] A. V. Afanasjev and O. Abdurazakov, Phys. Rev. C **88**, 014320 (2013).
[37] M. Baldo, L. M. Robledo, P. Schuck, and X. Viñas, Phys. Rev. C **87**, 064305 (2013).
[38] S. A. Giuliani and L. M. Robledo, Phys. Rev. C **88**, 054325 (2013).
[39] J. Dechargé and D. Gogny, Phys. Rev. C **21**, 1568 (1980).
[40] J. Bartel, P. Quentin, M. Brack, C. Guet, and H. B. Häkansson, Nucl. Phys. A **386**, 79 (1982).
[41] C. Wagemans, *The Nuclear Fission Process* (CRC Press, Boca Raton, FL, 1991).
[42] M. Brack, J. Damgaard, A. S. Jensen, H. C. Pauli, V. M. Strutinsky, and C. Y. Wong, Rev. Mod. Phys. **44**, 320 (1972).
[43] G. Bertsch and H. Flocard, Phys. Rev. C **43**, 2200 (1991).
[44] M. Girod and B. Grammaticos, Nucl. Phys. A **330**, 40 (1979).
[45] M. J. Giannoni and P. Quentin, Phys. Rev. C **21**, 2060 (1980); **21**, 2076 (1980).
[46] J. Libert, M. Girod, and J. P. Delaroche, Phys. Rev. C **60**, 054301 (1999).
[47] D. C. Hoffman, Nucl. Phys. A **502**, 21c (1989).
[48] J. M. Gates *et al.*, Phys. Rev. C **83**, 054618 (2011).
[49] Yu. Ts. Oganessian *et al.*, Phys. Rev. C **79**, 024603 (2009).
[50] Yu. Ts. Oganessian *et al.*, Phys. Rev. Lett. **104**, 142502 (2010).
[51] Yu. Ts. Oganessian *et al.*, Phys. Rev. Lett. **108**, 022502 (2012).
[52] H. Haba, D. Kaji, H. Kikunaga, Y. Kudou, K. Morimoto, K. Morita, K. Ozeki, T. Sumita, A. Yoneda, Y. Kasamatsu, Y. Komori, K. Ooe, and A. Shinohara, Phys. Rev. C **83**, 034602 (2011).
[53] J. Gerl, Acta Phys. Pol. B **40**, 767 (2009).
[54] L. Stavsetra, K. E. Gregorich, J. Dvorak, P. A. Ellison, I. Dragojević, M. A. Garcia, and H. Nitsche, Phys. Rev. Lett. **103**, 132502 (2009).
[55] R. Julin, Nucl. Phys. A **834**, 15c (2010).
[56] A. Sobiczewski and K. Pomorski, Prog. Part. Nucl. Phys. **58**, 292 (2007).
[57] U. Mosel and W. Greiner, Z. Phys. **222**, 261 (1969).
[58] M. Arnould, S. Goriely, and K. Takahashi, Phys. Rep. **450**, 97 (2007).
[59] V. E. Viola, Jr. and G. T. Seaborg, J. Inorg. Nucl. Chem. **28**, 741 (1966).
[60] A. Baran, Phys. Lett. B **76**, 8 (1978).
[61] A. Baran, J. A. Sheikh, J. Dobaczewski, W. Nazarewicz, and A. Staszczak, Phys. Rev. C **84**, 054321 (2011).
[62] F. Chappert, M. Girod, and S. Hilaire, Phys. Lett. B **668**, 420 (2008).
[63] S. Goriely, S. Hilaire, M. Girod, and S. Péru, Phys. Rev. Lett. **102**, 242501 (2009).
[64] R. Rodríguez-Guzmán, L. M. Robledo, and P. Sarriguren, Phys. Rev. C **86**, 034336 (2012).
[65] R. Rodríguez-Guzmán, P. Sarriguren, L. M. Robledo, and J. E. García-Ramos, Phys. Rev. C **81**, 024310 (2010).
[66] R. Rodríguez-Guzmán, J. L. Egido, and L. M. Robledo, Phys. Lett. B **474**, 15 (2000); Phys. Rev. C **62**, 054308 (2000).
[67] J. L. Egido and L. M. Robledo, Lect. Notes Phys. **641**, 269 (2004).
[68] L. M. Robledo, R. R. Rodríguez-Guzmán, and P. Sarriguren, Phys. Rev. C **78**, 034314 (2008).
[69] J. L. Egido, L. M. Robledo, and R. R. Rodríguez-Guzmán, Phys. Rev. Lett. **93**, 082502 (2004).
[70] R. R. Rodríguez-Guzmán, J. L. Egido, and L. M. Robledo, Phys. Rev. C **69**, 054319 (2004).
[71] J. F. Berger, M. Girod, and D. Gogny, Nucl. Phys. A **502**, 85c (1989).
[72] C. R. Chinn, J. F. Berger, D. Gogny, and M. S. Weiss, Phys. Rev. C **45**, 1700 (1992).
[73] J. L. Egido and L. M. Robledo, Nucl. Phys. A **494**, 85 (1989).
[74] J. L. Egido and L. M. Robledo, Phys. Rev. Lett. **70**, 2876 (1993).
[75] M. Girod, J. P. Delaroche, D. Gogny, and J. F. Berger, Phys. Rev. Lett. **62**, 2452 (1989).
[76] G. F. Bertsch, M. Girod, S. Hilaire, J. P. Delaroche, H. Goutte, and S. Péru, Phys. Rev. Lett. **99**, 032502 (2007).
[77] S. Péru, J. F. Berger, and P. F. Bortignon, Eur. Phys. J. A **26**, 25 (2005).

[78] R. Rodríguez-Guzmán, J. L. Egido, and L. M. Robledo, Nucl. Phys. A **709**, 201 (2002).
[79] R. Rodríguez-Guzmán, J. L. Egido, and L. M. Robledo, Phys. Rev. C **65**, 024304 (2002).
[80] S. Hilaire and M. Girod, Eur. Phys. J. A **33**, 237 (2007).
[81] J. P. Delaroche, M. Girod, J. Libert, H. Goutte, S. Hilaire, S. Péru, N. Pillet, and G. F. Bertsch, Phys. Rev. C **81**, 014303 (2010).
[82] R. Rodríguez-Guzmán, P. Sarriguren, L. M. Robledo, and S. Perez-Martin, Phys. Lett. B **691**, 202 (2010).
[83] L. M. Robledo, R. Rodríguez-Guzmán, and P. Sarriguren, J. Phys. G: Nucl. Part. Phys. **36**, 115104 (2009).
[84] R. Rodríguez-Guzmán, P. Sarriguren, and L. M. Robledo, Phys. Rev. C **82**, 061302(R) (2010).
[85] R. Rodríguez-Guzmán, P. Sarriguren, and L. M. Robledo, Phys. Rev. C **83**, 044307 (2011).
[86] L. M. Robledo and R. Rodríguez-Guzmán, J. Phys. G: Nucl. Part. Phys. **39**, 105103 (2012).
[87] B. Singh, R. Zywina, and R. Firestone, Nucl. Data Sheets **97**, 241 (2002).
[88] R. Capote *et al.*, Nucl. Data Sheets **110**, 3107 (2009).
[89] N. E. Holden and D. C. Hoffman, Pure Appl. Chem. **72**, 1525 (2000).
[90] L. Dematté, C. Wagemans, R. Barthélémy, R. Dhont, and A. Deruytter, Nucl. Phys. A **617**, 331 (1997).
[91] D. C. Hoffman and M. M. Hoffman, Annu. Rev. Nucl. Sci. **24**, 151 (1974).
[92] L. M. Robledo and G. F. Bertsch, Phys. Rev. C **84**, 014312 (2011).
[93] C. Titin-Schnaider and Ph. Quentin, Phys. Lett. B **49**, 213 (1974).
[94] M. Bender, K. Rutz, P.-G. Reinhard, J. A. Maruhn, and W. Greiner, Phys. Rev. C **58**, 2126 (1998).
[95] T. Dong and Z. Ren, Eur. Phys. J. A **26**, 69 (2005).
[96] G. Audi, A. H. Wapstra, and C. Thibault, Nucl. Phys. A **729**, 337 (2003).
[97] M. Warda and L. M. Robledo, Phys. Rev. C **84**, 044608 (2011).
[98] B. D. Wilkins, E. P. Steinberg, and R. R. Chasman, Phys. Rev. C **14**, 1832 (1976).
[99] H. Goutte, J. F. Berger, P. Casoli, and D. Gogny, Phys. Rev. C **71**, 024316 (2005).
[100] A. Mamdouh, J. M. Pearson, M. Rayet, and F. Tondeur, Nucl. Phys. A **679**, 337 (2001).
[101] K.-H. Schmidt *et al.*, Nucl. Phys. A **665**, 221 (2000).
[102] J. Sadhukhan, K. Mazurek, A. Baran, J. Dobaczewski, W. Nazarewicz, and J. A. Sheikh, Phys. Rev. C **88**, 064314 (2013).